Measurement report: Spatial variations in seasonal snowpack ionic chemistry and water stable isotopes across Svalbard

Elena Barbaro[1,2], Krystyna Koziol[3], Mats P. Björkman[4], Carmen P. Vega[5], Christian Zdanowicz[6], Tonu Martma[7], Jean-Charles Gallet[8], Daniel Kępski[9], Catherine Larose[10], Bartłomiej Luks[9], Florian Tolle[11], Thomas V. Schuler[12,13], Aleksander Uszczyk[14] and Andrea Spolaor[1,2]*

[1]Institute of Polar Sciences, ISP-CNR, Via Torino 155, 30170 Venice Mestre, Italy

[2]Department of Environmental Sciences, Informatics and Statistics, Ca' Foscari University of Venice, Via Torino 155, 30172, Venice, Italy.

[3]Department of Analytical Chemistry, Chemical Faculty, Gdansk University of Technology, G. Narutowicza 11/12, 80-233 Gdańsk, Poland.

[4]Department of Earth Sciences, University of Gothenburg, Box 460, SE-40530 Gothenburg, Sweden.

[5]Dirección Meteorológica de Chile, Dirección General de Aeronáutica Civil, Portales 3450, Santiago, Chile. *Previously at:* Department of Earth Sciences, Uppsala University, Villavägen 16, Uppsala, Sweden.

[6]Department of Earth Sciences, Uppsala University, Villavägen 16, SE-76236, Uppsala, Sweden.

[7]Department of Geology, Tallinn University of Technology, Ehitajate tee 5, 19086 Tallinn, Estonia

[8]Norwegian Polar Institute, Tromsø, No-9296, Norway

[9]Institute of Geophysics, Polish Academy of Sciences, Księcia Janusza 64, 01-452 Warsaw, Poland

[10]Environmental MicrobialGenomics, Laboratoire Ampère, CNRS, University of Lyon, France

[11]Université de Franche-Comté, Besancon, FEMTO-ST, UMR 6174 CNRS

[12]Departement of Geosciences, University of Oslo, Oslo, Norway

[13]Arctic Geophysics, University Centre in Svalbard, UNIS, Longyearbyen, Svalbard, Norway

[14]University of Silesia in Katowice, Faculty of Natural Sciences, Będzińska 60, 41-200 Sosnowiec, Poland

[*]**Corresponding author**

Andrea Spolaor (andrea.spolaor@cnr.it)

Keywords

Snow, Svalbard, Arctic, inorganic ions, water isotopes

Abstract

The Svalbard archipelago, located at the Arctic sea ice edge between 74° and 81° N, is ~60% covered by glaciers. The region experiences rapid variations in atmospheric flow during the snow season (from late September to May) and can be affected by air advected both from lower and higher latitudes, which likely impact the chemical composition of snowfall. While long-term changes in Svalbard snow chemistry have been documented in ice cores drilled from two high-elevation glaciers, the spatial variability of the snowpack composition across Svalbard is comparatively poorly understood. Here, we report the results of the most comprehensive seasonal snow chemistry survey to date, carried out in April 2016 across 22 sites on 7 glaciers across the archipelago. At each glacier, three snowpits were sampled along the altitudinal profiles and the collected samples were analysed for major ions (Ca^{2+}, K^+, Na^+, Mg^{2+}, NH_4^+, SO_4^{2-}, Br^-, Cl^- and NO_3^-) and stable water isotopes ($\delta^{18}O$, δ^2H). The main aims were to investigate the natural and anthropogenic processes influencing the snowpack and to better understand the influence of atmospheric aerosol transport and deposition patterns on the snow chemical composition. The snow deposited in the southern region of Svalbard is characterized by the highest total ionic loads, mainly attributed to sea salt particles. Both NO_3^- and NH_4^+ in the seasonal snowpack reflect secondary aerosol formation and post-depositional changes, resulting in very different spatial deposition patterns: NO_3^- has its highest loading in the northwestern Spitsbergen, and NH_4^+ in the southwest. The Br^- enrichment in snow is highest in northeastern glacier sites closest to areas of extensive sea ice coverage. Spatial correlation patterns between Na^+ and $\delta^{18}O$ suggest that the influence of long-range transport of aerosols on snow chemistry is proportionally greater above 600-700 m a.s.l.

1. Introduction

Svalbard is a region of the Arctic experiencing rapid climate change. The mean warming rate is +1.35 K per decade, much faster than the global average (Isaksen et al., 2016; Maturilli et al., 2013; Nordli et al., 2014). This archipelago is located at the southern edge of the perennial Arctic sea ice in the North Atlantic Ocean, and is characterized by a maritime climate with large, rapid temperature variations during winter (Brage et al., 2014). South-westerly inflow of mild oceanic air, associated with a low-pressure system east of Iceland, often brings relatively warm and moist air in the winter months, while Arctic air intrusions from the north-east, driven by a high-pressure system over Greenland, result in much colder temperatures (Rinke et al., 2017). In addition to these synoptic fluctuations, intense autumn or winter cyclonic storms associated with anomalous warming events sometimes occur, transporting both heat and moisture from lower latitudes to Svalbard (Rinke et al., 2017).

The aforementioned meteorological conditions also favor long-range transport of aerosols to the archipelago, including pollutants from continental sources. Depending on the predominant air flow pattern at the time of snowfall, the archipelago may experience regionally different amounts of both snow accumulation (Eneroth et al., 2003; Forland et al., 2011) and chemical loads, the latter reflecting

contrasting mixtures of aerosols, varying by source area (Aas et al., 2016; Forsström et al., 2009; Möller and Kohler, 2018). These regional differences are also associated with contrasts in sea ice cover. While all Svalbard coasts are usually ice-free in summer, sea ice can form and cover large parts of the ocean surface in the eastern and northern parts of the archipelago. Contrastingly, the southern and western parts often remain ice-free (Dahlke et al., 2020), and therefore tend to experience greater snowfall owing to the proximity of open water. In addition, the West Spitsbergen Current, a branch of the Atlantic Meridional Overturning Circulation (AMOC) that flows to the west of the archipelago, causes markedly different regional climatic conditions between its eastern and western parts (van Pelt et al., 2019): the west exhibits higher temperatures and precipitation, while the east is less humid and cooler, and has also experienced a stronger warming trend since 1957.

The seasonal snowpack contains a complex mixture of impurities that are either scavenged from the atmosphere during snowfall or directly received through dry deposition (Kuhn, 2001). On land, the majority of impurities found in seasonal snow are usually eluted during summer melting, influencing terrestrial and aquatic systems (Björkman et al., 2014; Brimblecombe et al., 1987). However, in the accumulation area of Arctic glaciers and ice caps, impurities can be retained within or below the seasonal snow layer (Björkman et al., 2014; Pohjola et al., 2002; Vega et al., 2015b). For this reason, chemical impurities such as major ions (Ca^{2+}, K^{+}, Na^{+}, Mg^{2+}, NH_4^{+}, $SO4^{2-}$, Br^{-}, Cl^{-} and NO_3^{-}) in ice cores have been widely used to study the past trends of atmospheric and climatic conditions (Barbante et al., 2017; Isaksson et al., 2003; Thompson et al., 2002; Wolff et al., 2010). Previous studies in Svalbard (Isaksson et al., 2001; Matoba et al., 2002; Nawrot et al., 2016; Semb et al., 1984) have shown that the chemistry of the seasonal snowpack is dominated by sea salt ions (Hodgkins and Tranter, 1998). However, the region is also a sink for atmospheric contaminants brought in by long-range transport (Vecchiato et al., 2018). Investigations of precipitation and snow cover chemistry have predominantly focused on the central and western parts of the archipelago (Kühnel et al., 2011; Nawrot et al., 2016; Vega et al., 2015a; Virkkunen et al., 2007), due to the accessibility of research facilities in these sectors.

In general, stable water isotope measurements in different components of the water cycle are available in isotope databases, maintained and updated by the International Atomic Energy Agency (IAEA), but also by national or international organizations (Jason B. West et al., 2010). Moreover, in Svalbard, stable water isotope investigations are performed in ice cores and surface snowpits samples because $\delta^{18}O$ and $\delta^{2}H$ are still the most common tools for finding the depth/time relation in ice cores (Pohjola et al., 2017; Punning et al., 1986). The preservation of un-interrupted annual isotope cycles varies depending on the site: in sites with excellent environmental conditions such as central Greenland, while in sites with high intra-seasonal variation or with different pre- and post-depositional processes the annual layers can be difficult to distinguish (Igarashi et al. 2001). To investigate to what degree $\delta^{18}O$ in snow changes after accumulation, carried out the observation of the precipitation at Ny-Ålesund. These authors concluded that the fluctuation of $\delta^{18}O$ couldnot be explained by changes in surface air temperature only, but that the

characteristics of the air masses also influenced the isotope signature of the precipitation (Igarashi et al., 2001).

In the present study, the concentration, mass loading, spatial and altitudinal distribution of major ion species (Ca^{2+}, K^{+}, Na^{2+}, Mg^{2+}, NH_4^{+}, SO_4^{2-}, Br^{-}, Cl^{-} and NO_3^{-}) in snow, together with its stable oxygen and hydrogen isotope composition ($\delta^{18}O$ and $\delta^{2}H$), were evaluated in the late winter snowpack at 22 glacier sites across Svalbard. Stable isotope ratios were used as supporting data to define the accumulation seasonality in snowpack, and to identify the moisture sources that feed snowfall, thereby providing clues to the predominant air transport pathways to the snowpit sites (Gat et al., 2001).This study was part of the larger Community Coordinated Snow Study in Svalbard (C2S3) project and the most comprehensive survey of seasonal snow chemistry in Svalbard to date. The snowpack survey, which was carried out by coordinated teams using a common sampling protocol (Gallet et al., 2018), aimed to map and characterize regional differences in the chemical composition and impurity load of the winter snowpack. We further interpret the observed differences in chemical loading in relation to meteorological and other environmental factors.

Thereby, we aim to identify the conditions controlling the chemistry of Svalbard snow that are susceptible to the variable climate warming impact across the region.

2. Methods

2.1 Sampling location and strategy

During April 2016, the seasonal snowpack was sampled at 22 sites on seven glaciers across Svalbard (Table 1 and Figure 1). The glaciers are of different sizes and hypsometry. Wind fields for each glacier are not available. Indeed the wind direction can change in concomitance with cyclonic events that could occur during the season and can act differently for each glacier.

The first glacier considered in this study is Austfonna (AF), located on Nordaustlandet, the second largest island in Svalbard, with approximately 80% of its area covered by ice. AF is the largest icecap in Svalbard with a geographic area of 8357 km^2 and one main central dome of up to 600 m ice thickness feeding several drainage basins (Dallmann, 2015; Schuler et al., 2020).

The other six glaciers investigated here are located on the Spitsbergen Island. On the northwestern Spitsbergen, we studied three glaciers near Ny-Ålesund: Austre Lovénbreen (ALB), Kongsvegen (KVG), and Holtedahlfonna (HDF). ALB is a small land-based valley glacier, 4 km long from south to north along the Brøgger Peninsula. The glacier area was 4.48 km^2 in 2013 and its elevation ranges from 50 to 550 m a.s.l. The total catchment area spreads over 10.577 km^2, taking into account an outlet where the main stream crosses a compact calcareous outcrop 400m upstream from the coastline (Marlin et al., 2017). KVG is a northwest-flowing grounded glacier located about 20 km east of Ny-Ålesund (Melvold & Hagen 1998), with an average ice thinness of 190 m and maximum 450m (Lindbäck et al., 2018) It has a total length of ca. 24 km with an average 3.5 km width, has a maximum elevation of 800 m a.s.l. and flows from south-east to north-west (Spolaor et al., 2017). HDF glacier is the largest ice field (c.a. 300

147 km^2) on the northwestern Spitsbergen Island, about 40 km from the Ny-Ålesund station. It is distributed
148 over an elevation range of 0–1241 m a.s.l (Beaudon et al., 2017; Nuth et al., 2017).
149 Lomonosovfonna (LF) is one of the highest ice fields on Spitsbergen and it is located on the central part
150 of island. The summit lies at 1250 m a.s.l. and has a pronounced cupola shape with an approximate
151 radius of 500 m and a total he accumulation area of the entire LF ice system was about 600 km^2 in the
152 beginning of the 21st century (Isaksson et al., 2001). Even though this is the highest point in our survey,
153 the air temperature here can pass above zero during the summer with relocation, although not significant,
154 of ions as a result(Pohjola et al., 2002; Vega et al., 2016). In southern Spitsbergen, two different glaciers
155 were investigated, Hansbreen (HB) and Werenskiöldbreen (WB), close to the Hornsund station. The HB
156 is a medium-sized (56 km^2) tidewater glacier located in the southern part of Wedel Jarlsberg Land. The
157 glacier is ~16 km long, and its elevation extends up to 550 m a.s.l. The WSB glacier has an area of 27
158 km^2, is a land-terminating valley glacier to the west of HB, and ranges in elevation from 50 to 600 m
159 a.s.l.(Schuler et al., 2020).
160 Each glacier was sampled in the ablation zone, close to the equilibrium line altitude (ELA), and in the
161 accumulation zone (Table 1). The ELA is the elevation at which the surface mass balance is zero, i.e.,
162 where the accumulation of snow is exactly balanced by ablation over a period of a year (Cogley et al.,
163 2011). Although the exact elevation ranges of these zones (accumulation, ablation, and ELA) differ for
164 each glacier, they share enough glaciological similarities to support intersite comparisons.
165
166 ***2.2. Sampling procedure***
167 Snowpit sampling was performed using a common protocol (Gallet et al., 2018) with pre-cleaned
168 equipment (i.e., tubes, plastic scrapers, and plastic shovels cleaned with ultrapure water) and protective
169 clothing (powder-free plastic gloves, clean suits and face masks). This protocol allowed sampling and
170 field data collection in a consistent manner, obtaining comparable datasets from different research sites.
171 Samples for ionic chemistry were taken from each discrete snow pit layer, according to the visible
172 stratigraphy, and directly into pre-cleaned, 50 mL polypropylene "Falcon" centrifuge tubes. This type of
173 sampling facilitates linking a snow layer (and its properties) to a specific weather event (i.e., precipitation
174 or surface melt). Moreover, sampling by discrete layers makes it possible to correlate the intervals of
175 snow accumulation between separate snow pits at different altitudes, as reported in this paper when we
176 compared three different areas in the same glacier (ablation, ELA and accumulation). It is also more
177 accurate for chemical load calculations where ice layers occur in snow pits.
178 Samples for the isotopic composition of water were collected at a 5-cm resolution for sites in the Ny-
179 Ålesund area and at a 10-cm or stratigraphic layer resolution for other sites. All sampling was conducted
180 at a safe distance and upwind from potential local pollution sources, such as the snowmobiles used for
181 transport by the sampling team.
182
183 ***2.3 Major ion analyses***

Samples from glaciers in the Hornsund area (HB, WB) were analysed at the Polish Polar Station Hornsund (Institute of Geophysics, Polish Academy of Sciences), while samples from glaciers near Ny-Ålesund (KVG, ALB, HDF) were shipped frozen to the Institute of Polar Sciences (ISP-CNR) in Venice (Italy). Snow sampled in central Spitsbergen (AF, LF) was shipped frozen to the Department of Earth Sciences at Uppsala University (Sweden). Due to a temporary equipment malfunction in Uppsala, only cations could be analysed there, and the refrozen samples were forwarded to ISP-CNR for anion analysis. All samples and standards were handled and prepared under clean room conditions, wearing powder-free gloves. In all labs except at the Polish Polar Station Hornsund, laminar flow hoods (class 100) were used. Samples were melted immediately before analysis.

2.3.1. Hornsund

Samples were filtered through 0.45 µm mixed cellulose esters membranes (Merck Millipore S-pak®) prior to analysis. Ion concentrations were determined on a Metrohm 761 Compact IC ion chromatograph equipped with an autosampler (Metrohm, Herisau, Switzerland), with isocratic flow of 0.69 mL min^{-1}, and chemical suppression for anions (column Metrosep A Supp S + Metrosep A Supp 4/5 Guard 4.0, eluent: $NaHCO_3$ 1.0 mmol L^{-1} + Na_2CO_3 3.2 mmol L^{-1}). Cations were determined without suppression (column Metrosep C4 + Metrosep C4 Guard; mobile phase: HNO_3 1.7 mmol L^{-1} + 2,6-pyridinecarboxylic acid [dipicolinic acid, DPA] 0.7 mmol L^{-1} at a flow rate of 0.9 mL min^{-1}). Cation samples were acidified with 2 µL of 2mM HNO_3 per 10 mL sample prior to analysis. The injection volume was 20 µL in the anion system and 100 µL in the cation system. Nitric acid solutions were prepared from POCH S.A. (Poland) concentrated weighed amounts, while sodium carbonate and hydrogen carbonate as well as DPA were dissolved from the solid phase (Merck Millipore).

2.3.2 Uppsala

Samples were filtered using 0.22 µm polyethersulfone membranes (Minisart®, Sartorius) and cation determination was performed using a Metrohm ProfIC850 ion chromatograph (Metrohm, Herisau, Switzerland), equipped with an autosampler and a Metrosep C4 column. The mobile phase of 0.02 M DPA and 0.1 M HNO_3 was run in isocratic flow of 0.7 mL min^{-1}. Very low detection limits (≤ 0.006 mg $^{-1}$L) were achieved thanks to the sample injection volume of 500 µL.

2.3.3. Venice

Anion determination was performed using a Dionex™ ICS-5000 ion chromatograph (ThermoScientific™, Waltham, US) equipped with an anionic exchange column (Dionex IonPac AS 11, 2 × 250 mm) and a guard column (Dionex IonPac AG11 2 × 50 mm). Sodium hydroxide (NaOH), used as a mobile phase, was produced by an eluent generator (Dionex ICS 5000EG, Thermo Scientific). The gradient with a 0.25 mL min^{-1} flow rate was 0 min, 0.5 mM; 0–3.5 min, gradient from 0.5 to 5 mM; 3.5–5 min, gradient from 5 to 10 mM; 5–25 min, gradient from 10 to 38 mM; 25–30 min, column cleaning

with 38 mM; 30–35 min; equilibration at 0.5 mM. The injection volume was 100 µL. The IC was coupled to a single quadrupole mass spectrometer (MSQ Plus™, Thermo Scientific™) with an electrospray source (ESI) that operated in negative mode. All other details are reported by (Barbaro et al., 2017).

To determine the cations, a capillary ion chromatograph (Thermo Scientific Dionex ICS-5000) equipped with a capillary cation exchange column (DionexIonPac CS19-4µm, 0.4 × 250 mm) and a guard column (Dionex IonPac CG19-4µm, 0.4 × 50 mm) and coupled to a conductivity detector was used. Methanesulfonic acid, produced by an eluent generator (Dionex ICS 5000EG, Thermo Scientific), was applied as mobile phase. The gradient was 0 – 17.3 min: 1.5 mM; 17.3 – 21.9 min: from 1.5 to 11 mM; 21.9–30 min: equilibration at 1.5 mM. The injection volume was 0.4 µL and the flow rate was 13 µL min^{-1}.

2.3.4. Instrumental performance of each laboratory

For all laboratories, calibrations for ions were evaluated using analytical standards (Merck/Sigma Aldrich). The calibrations in each lab delivered different linear ranges for each ion due to the different methods used (Table S1). Good linearity was demonstrated in each lab and all calibration curves had R^2 > 0.99. Samples that had ion concentrations beyond the calibration range were diluted with ultrapure water before re-analysis. Analytical blanks of ultrapure water (>18 MΩ cm) were included in the analysis at all three labs. The method detection limit (MDL) was set to three times the standard deviation of the blank values (Table S1). For Na^+, Mg^{2+}, Cl^- and SO_4^{2-}, values < MDL occurred in less than 10% of cases, and for Ca^{2+} and NO_3^- the < MDL concentrations were noted in 12% and 17% of all cases, respectively. However, K^+ and Br^- were detected only in 53% and 46% of all samples, respectively, while NH_4^+ concentration exceeded the MDL only in 36% of all measurements. For the calculation of the bulk ionic loading in snowpits, values < MDL were assumed to be equal to half the MDL.

Accuracy and precision are important parameters to evaluate during method validation. Checks for accuracy were made using certified multi-element standard solutions for anions (F^-, Cl^-, Br^-, NO_3^-, SO_4^{2-}, n° 89886-50ML-F, Sigma Aldrich) and cations (Na^+, K^+, Mg^{2+}, Ca^{2+}, n° 89316-50ML-F, Sigma Aldrich), at the concentration of 10 mg L^{-1} ± 0.2%. Accuracy is expressed as a relative error calculated as (Q−T)/T×100, where Q is the determined value and T is the "true" value. The accuracy for each ion in all labs was always <±10%, except for Mg^{2+} measurements at the Hornsund laboratory. The analytical precision was quantified as the relative standard deviation (RSD) for replicates (n > 3) of standard solutions and was always < 10% for each ion (Table S1).

2.4. Stable water isotopes

The determination of stable isotope ratios of O and H was performed at Tallinn University of Technology (Estonia). The isotopic ratios were determined by laser spectroscopy, using a Picarro model

L2120-i water isotope analyzer (Picarro Inc., Sunnyvale, USA), which allows for the simultaneous determinations of $^{18}O/^{16}O$ and $^{2}H/^{1}H$ in H_2O with a high-precision AO211 vaporizer. Results are reported in the standard delta notation as $\delta^{18}O$ and $\delta^{2}H$ relative to Vienna Standard Mean Ocean Water (VSMOW). Reproducibility was ±0.1‰ for $\delta^{18}O$ and ±1‰ for $\delta^{2}H$, respectively. 7 injections were carried out for each sample, but only the last 4 injections (4 to 7) were used for calculations to minimize the memory effect. Laboratory standards TLN-A2 (-10.15; -77.5) and TLN-B2 (-21.95; -162.5) were regularly calibrated against international V-SMOW, GNIP and V-SLAP standards. Standards (TLN-A2, TLN-B, and TLN-D4) were measured at the beginning, in the middle, and at the end of each set of measurements (54 bottles). Additionally, every 7 samples, the laboratory standard TLN-D4 (-17.5; -133.0) was measured and used for drift correction if needed.

3. Results

3.1 Spatial distribution of ionic species

To investigate differences in snowpack composition across all glaciers, we compared the total mass of ions that accumulated in snow at the different sampling sites. On average, the snow cover season on Svalbard lasts from early September to early May, but snow may also fall in summer months at high elevations. The snow pits in this study were sampled in early to late April 2016 and therefore might not contain the full annual ionic burden, since deposition can still occur before the began of the snow melting. Therefore, we report these data as ionic loads (mg m^{-2}) rather than annual fluxes. In each snow pit, the total ionic load was calculated as the cumulative sum of the ionic loads in each discrete layer, i.e., ionic concentrations multiplied by the snow water equivalent of the layer (Table 2). On the other hand, to evaluate the transport processes of chemical species from the other regions to Svalbard, we evaluate the volume-weighted mean concentrations of major ions in each snow pit. These values are calculated as the total ionic load of each snow pit divided by its total SWE (snow water equivalent) (Table 3). The snowpack chemical characteristics were then compared between glacier zones (ablation zone, ELA, and accumulation zone; Figure 1).

Snow pit samples collected in the Hornsund area (HB and WB, southern Spitsbergen) show a markedly higher total load for all major ions (Figures 1 and 2) than at all other sites. The samples collected in the accumulation zones of WB and HB have total ionic loads of 8161 and 8023 mg m^{-2}, respectively, four times higher than those collected in the accumulation zone of KVG (2861 mg m^{-2}), AF (2607 mg m^{-2}) and ALB (1934 mg m^{-2}) and 16 times higher than those sampled at LF (639 mg m^{-2}) and HDF (583 mg m^{-2}). Similar differences are observed for the snowpits collected at lower altitudes (Figure 2).

In the accumulation zone of all glaciers (Figure 3), Na^{+} and Cl^{-} are generally the most abundant ionic species, with percentages ranging from 29% (HDF) to 36% (AF) for Na^{+}, and from 34% (LF) to 48% (HB and WB) for Cl^{-}, respectively. The snowpack on Hornsund glaciers (HB, WB) has higher Cl^{-}

293 percentages (48–49%) compared to that of other glaciers (34–39%), while conversely the SO_4^{2-}
294 percentage is lower there (9%) than on other glaciers (11–23%). The ionic loads are generally highest in
295 the accumulation zone of glaciers and lowest in the ablation zone (Figure 2), mostly due to the lower
296 snow accumulation. This pattern holds true for Na^+, Cl^-, NH_4^+, K^+, Ca^{2+}, and Mg^{2+} at most glacier sites,
297 except in the Hornsund area. The load of Br^- is similar on glaciers of the Ny-Ålesund sector (ALB, HDF,
298 KVG) and on LF, but is higher in AF and Hornsund glaciers (HB, WB; Figure 2). The load of NO_3^- is
299 similar for all glaciers, except for LF, where very low loads are found. Unlike total SO_4^{2-}, the non-sea-
300 salt fraction of sulphate (nss-SO_4^{2-}), calculated using a seawater SO_4^{2-}:Na^+ mass ratio of 0.252 (Millero et
301 al., 2008), shows lower loads on Hornsund glaciers (15–107 mg m^{-2}) when compared to glaciers in other
302 parts of the archipelago (Figure 1, Table 2). The nss-SO_4^{2-} loads vary between 22–131 mg m^{-2} at HDF
303 and LF, 75–266 mg m^{-2} at KVG and ALB, and 153–206 mg m^{-2} at AF.
304
305 ***3.2 Stable water isotopes ($\delta^{18}O$ and δ^2H)***
306 Our results provide the first picture of spatial variations in the mean stable water isotope composition of
307 the seasonal snowpack across Svalbard (Table 2, Figure 4). The SWE-weighted mean $\delta^{18}O$ and δ^2H are
308 calculated using the formula SWE-$\delta = \sum(\delta_i \times SWE_i)/SWE_t$ where δ_i are the δ values of each layer, SWE_i
309 are SWE of each layer and SWE_t is the SWE of the entire snowpit. These SWE-weighted mean values
310 decrease significantly from south to north (Spearman rank correlation ρ with latitude is -0.69 and -0.65
311 for $\delta^{18}O$ and δ^2H, with $p < 0.001$ and $p < 0.01$, respectively). The isotopically heaviest snow (least
312 negative δ values) occurs on glaciers of the Hornsund area ($\delta^{18}O$: -11.25 to -9.54 ‰; δ^2H: -77.62 to -
313 63.64 ‰), and the isotopically lightest (most negative δ values) in AF ($\delta^{18}O$: -16.00 to -13.89 ‰; δ^2H: -
314 111.15 to -96.89 ‰). Glacier sites in NW Spitsbergen (KVG, ALB, and HDF) and on LF have mean
315 $\delta^{18}O$ and δ^2H values that fall within these ranges. On KVG, ALB, HDF and LF, the $\delta^{18}O$ and δ^2H in
316 snow decrease monotonically (becoming gradually more negative) with increasing elevation. On the
317 other hand, AF, WB, and HB there was no statistical difference between the mean $\delta^{18}O$ and δ^2H values
318 (Figure 4). A general significant anticorrelation with altitude was found for SWE-weighted mean δ^2H (ρ
319 = -0.63, $p < 0.01$), and $\delta^{18}O$ (ρ = -0.65, $p < 0.01$).
320
321 **4. Discussion**
322
323 There have been few published studies on recent seasonal snow or firn chemistry in Svalbard, hence
324 comparisons of our data with these earlier results are limited to a few sites. (Virkkunen et al., 2007) and
325 (Vega et al., 2015a) quantified the annual chemical loads of Na^+, Ca^{2+}, NO_3^- and nss-SO_4^{2-} at
326 Lomonosovfonna summit (LF3) from 2002 to 2011 using snow and firn cores. In Table 4, we also report
327 the unpublished data of samples collected in 2009-2011 by C. Vega, obtained using the methods outlined
328 in Section 2.2. Our study extends these data to 2016. The range of annual ionic loads at LF3 over the 15-
329 year period is wide, and no clear temporal trend can be identified (Table 4). At Holtedahlfonna summit

(HDF3), firn core measurements by (Spolaor et al., 2013) found a mean Na^+ concentration of 110 ± 73 ng g^{-1} over the period 2003-2012, while the mean concentration in the April 2016 snowpack (this study) was 191 ng g^{-1}, hence within the range reported in earlier years.

4.1 The main ion sources in the seasonal snow of Svalbard

The composition of the Svalbard seasonal snowpack sampled during the C2S3 project clearly indicates that the ocean is the main source of ions in snow, as was shown by Hodgkins and Tranter (1998). At all sites, the dominant ions are Na^+, Cl^-, and SO_4^{2-}, with comparatively minor amounts of K^+, Ca^{2+}, and Mg^{2+} (Figure 3). To help clarify the possible sources and modes of deposition of ions in snow, we computed Spearman rank correlations between total ionic loads (ρ_{load}), as well as between volume-weighted mean ionic concentrations (ρ_{conc}), across all snowpits (n = 22; Table 5). The chemical species that are predominantly wet-deposited, sharing common sources and not undergoing significant composition changes in transport should exhibit similar concentration patterns (high ρ_{conc}) (Schüpbach et al., 2018). The concentrations of Mg^{2+}, K^+, and Ca^{2+} were all positively correlated with those of Na^+ and Cl^-, indicating a common sea spray source. Moreover, this input was the single significant source of K^+ and Mg^{2+}, as indicated by near-zero calculated values of nss-K^+ and nss-Mg^{2+} in the sampled snowpits (Table 3). The ρ_{load} correlations are very similar for these ionic species, which points to both wet and dry deposition being a significant mechanism in their accumulation in the snowpack.

The concentrations of Mg^{2+} are positively and significantly correlated with both Ca^{2+} and nss-Ca^{2+} (ρ_{conc} = 0.70 and 0.47, respectively; the latter coefficient was higher for loads at 0.56; Table 5), suggesting that they share some non-marine source(s). Furthermore, all glaciers have greater Ca^{2+}:Mg^{2+} ratios than seawater (0.32; (Millero et al., 2008), Figure 5). It is likely that the excess Ca^{2+} and Mg^{2+} come from mineral particles, i.e., $CaCO_3$ (calcite) and $CaMg(CO_3)_2$ (dolomite), derived from local rock (or soil) dust (Kekonen et al., 2005), especially limestone, dolostone and marble, which are abundant in Svalbard (Dallmann, 1999). The presence of carbonate ions in the collected snow samples would explain the missing negative charge in the ionic balance (anion X^-; Figure S1).

Sulphate (SO_4^{2-}) is highly and significantly correlated ($p < 0.05$) with both Na^+ (ρ_{load} = 0.92; ρ_{conc} = 0.80) and Cl^- (ρ_{load} = 0.93; ρ_{conc} = 0.75), indicating that sea spray is its main source. However, Na^+/SO_4^{2-} and Cl^-/SO_4^{2-} ratios are well below seawater values (Millero et al., 2008) on most glaciers except for those near Hornsund (WB and HB), suggesting input of nss-SO_4^{2-} (Figure 5). Biogenic nss-SO_4^{2-} can occur in snow as an oxidized by-product of dimethyl sulphide (DMS) emitted by marine algal blooms (Gondwe et al., 2003), typically initiated in April but sometimes later (Ardyna et al., 2013). Another plausible source of nss-SO_4^{2-} deposition in Svalbard is long-range atmospheric transport of secondary aerosols containing SO_4^{2-}, such as ammonium sulfate. This sulphate can be formed by SO_x emitted from coal combustion

throughout the winter and biomass burning in the spring (Barrie, 1986; Law and Stohl, 2007; Nawrot et al., 2016). The nss-SO_4^{2-} does not correlate significantly with other ionic species, suggesting a separate origin. However, we need to caution that in the southern region of Svalbard, the estimation of ss-SO_4^{2-} is subject to higher uncertainty because of the higher amount of Na^+ in the atmospheric deposition there.

Bulk ionic loads of SO_4^{2-} in the snowpits were significantly and positively correlated with those of NO_3^- (ρ_{load} = 0.55) and NH_4^+ (ρ_{load} = 0.68), but the correlations between weighted mean ionic concentrations were not significant, hinting at co-deposition (wet) rather than shared sources (Table 5). These species are known to form secondary aerosols (Karl et al., 2019; Schaap et al., 2004) and thus their proportions in aerosols may differ significantly from those in their source emissions. It is also possible that nitrogen species underwent further post-depositional photochemical reduction and evasion, thereby reducing their concentrations in snow (Curtis et al., 2018). Finally, we remark here that the snowpit sampling was done in April, earlier than the beginning of the oceanic algal bloom in the surrounding Svalbard basin, which could have led to an underrepresentation of biological emissions from late spring in our samples.

Spatial variations of ammonium load (NH_4^+) across Svalbard glaciers mirrored the pattern shown by sea salt ions, with higher loads in the Hornsund area and lower loads in other areas. This was also reflected by significant correlations between the bulk loads of NH_4^+ with those of Na^+ and Cl^- (ρ_{load} = 0.64 and 0.73, respectively), and with Na^+, K^+ and Mg^{2+} by concentration (ρ_{conc} = 0.47, 0.62 and 0.47, respectively). Ammonium has been linked to biogenic, forest fire, and anthropogenic agricultural emissions (Trachsel et al., 2019). The higher annual snowpack load of NH_4^+, determined in the Hornsund area is more likely connected with biological sources than anthropogenic activities, although some contribution from biomass burning events cannot be excluded. The marine primary productivity in spring 2016 (April and May) was higher in the south-eastern ocean sector of the Svalbard archipelago (Figure S2), which could partially explain the higher NH_4^+ load. This would also explain the correlation between ammonium and sea-salt ions (Table 5). Locally, especially for HB, there may be extra NH_4^+ emissions from bird colonies (Keslinka et al., 2019; Wojczulanis K. et al., 2008).

Unlike NH_4^+, the bulk loading of NO_3^- in snow was highest in northwestern Spitsbergen (Ny-Ålesund area), when compared to other parts of Svalbard. Deposition of NO_3^- in Arctic snow is often associated with the long-range atmospheric transport of NO_x and related N species from anthropogenic source regions at lower latitudes (Björkman et al., 2014; Fibiger et al., 2016; Vega et al., 2015a). Differences in NO_3^- loads in snow in various parts of Svalbard might therefore reflect differences in the transport pathways of precipitating air masses, including the formation of secondary aerosols, or post-depositional processes, rather than local emissions. While local shipping routes and the settlement of Ny-Ålesund itself may contribute NO_3^- emissions (Winther et al., 2014), the highest share of the total ionic load of NO_3^- was found in the accumulation zone of HDF (9% of the total ionic load; Figure 3). Given that HDF

is the most remote site from Ny-Ålesund relative to KVG or ALB, it should not capture a high share of local pollution. The highest correlation coefficient for NO_3^-, both in terms of concentrations and loads, was found with nss-Ca^{2+}. This would support both the formation of calcium nitrate in the atmosphere (Gibson et al., 2006) or post-depositional processes removing the NO_3^- from layers poor in Ca^{2+}, since calcium has been hypothesised to stabilise the nitrate in snowpack against post-depositional losses (Kekonen et al., 2017).

4.2. Chlorine depletion

Although Na^+ and Cl^-, the main species of sea salt, were significantly correlated (ρ_{conc} = 0.95), the values of the Cl^-/Na^+ ratio in snow were lower than that in seawater on most studied glaciers, except those near Hornsund (Figure 5), suggesting a Cl^- deficit at the more northerly sites. Whillow et al. (Whitlow et al., 1992) found an opposite situation in the snowpack of Greenland, indicating Cl^-/Na^+ values higher than the ratio of seawater. This Cl^- enrichment relative to the Cl^-/Na^+ ratio in seawater may reflect Cl derived from anthropogenic sources as well from gas phase chlorine transportation and deposition in central Greenland.

Contrastingly, a possible explanation of Cl^- deficit in the Svalbard snowpack might be de-chlorination of the sea spray aerosol during transport or, less likely, at the snow-atmosphere interface. This reaction occurs between sea salt particles, containing NaCl, and HNO_3, H_2SO_4, or organic acids to release gaseous HCl (Zhuang et al., 1999). We calculated the percentage of Cl^- depletion (Cl^-_{dep}) as $Cl^-_{dep} = (Cl^-_{ss} - Cl^-_{meas}) / Cl^-_{ss} \times 100\%$, where $Cl^-_{ss} = 1.174\ Na^+_{meas}$, and Cl^-_{meas} and Na^+_{meas} are the measured equivalent concentrations (Yao et al., 2003). Except for site HDF2 (Cl^-_{dep} = 2%), the lowest mean Cl^-_{dep} values were obtained for Hornsund glaciers (WB, HB: 10–19%), while values at other glacier sites ranged between 21 and 75% (Table 2). This suggests that sea-salt aerosols travel along a route from southern to northern Svalbard, which gives more time for Cl^- depletion in the ionic mixtures reaching locations that are more northerly.

4.3. Bromine enrichment

In addition to Cl^-, snowfall can scavenge Br^- (Peterson et al., 2019; Spolaor et al., 2019). Br^- loads on Svalbard glaciers surveyed in April 2016 were positively and significantly correlated with those of primary sea salt ions Na^+ (ρ_{load} = 0.48), Cl^- (ρ_{load} = 0.53) and Mg^{2+} (ρ_{load} = 0.51) (Table 5). Correlations between weighted mean concentrations were not significant, however, suggesting departures of the Br^- concentrations in snow from typical seawater ionic ratios at some glacier sites. A Br^- enrichment factor (Br_{enr}) can be calculated as $Br_{enr} = Br^- / (0.0065\ Na^+)$, where 0.0065 is the Br^- : Na^+ seawater mass ratio (Maffezzoli et al., 2017). The Br_{enr} reflects specific processes (in particular sea ice Br emission) that affect the Br^- concentration and load in the snowpack (Spolaor et al., 2014). Results of our calculations (Table 2, Figure S3) show that for glaciers of the Hornsund area (HB and WB) and NW Spitsbergen (KVG, ALB and HDF), the mean Br_{enr} values are often < 1, indicating some Br^- depletion, in agreement

with the findings of (Jacobi et al., 2019) for glaciers in the Ny-Ålesund area. The depletion could be a result of snowpack Br re-emission, but this seems unlikely since field measurements near Ny-Ålesund found no evidence of such volatilization of snow-bound Br (Spolaor et al., 2019).

Alternatively, Br^- depletion could occur through BrO loss from marine aerosols and subsequent deposition of these Br-depleted aerosols in snow. In contrast to southern and northwestern Spitsbergen, glaciers in central Spitsbergen (LF) and in Nordaustlandet (AF), showed Br_{enr} values > 1. These glaciers lie relatively close to areas to the east of the archipelago that are often covered by first-year sea ice. Newly-formed sea ice has been shown to release gas phase Br into the polar atmosphere, thus supplying an extra Br source in addition to sea spray (Spolaor et al., 2016). The spatial distribution of the Br-enriched snowpit sites supports this, i.e., the sites closest to the areas covered by first-year sea ice have the largest Br enrichments, and the latter decrease with greater distance from the eastern shores of Svalbard (Figure S3). A survey of the average sea-ice coverage in the period March – May 2016, which is relevant to the Br enrichment phenomenon, confirms that the north-eastern and eastern shore of Svalbard were indeed covered much more frequently by close and open drift ice than the south or north-west (data from Norwegian Meteorological Institute).

4.4 Distribution pattern of $\delta^{18}O$ and $\delta^{2}H$

As described earlier, the SWE-weighted mean $\delta^{18}O$ and $\delta^{2}H$ values in glacier snowpits decreased significantly with increasing latitude across Svalbard, the least negative values occurring on glaciers of the Hornsund area, and the most negative in Austfonna (Table 2). This pattern follows the climate gradient across the archipelago, milder in the south, colder in the north. Part of the south-north contrast in δ values could be explained by the lower mean altitude of glacier sites in the Hornsund area compared to some of the higher-elevation sites further north on Spitsbergen or on Austfonna, and the relationship with elevation was similar for both isotopic ratios in the collected dataset.

Deuterium excess ($d = \delta^{2}H-(8\cdot\delta^{18}O)$) is mainly influenced by the source region of the precipitating moisture and in particular by the sea surface temperature, but also relative humidity and wind speed (Gat, 1996; Uemura et al., 2008). In addition, d is also influenced by the temperature gradient between the moisture source and precipitation area (Johnsen et al., 1989). The SWE-weighted mean d values in Svalbard snowpits varied within a relatively narrow range of 6.74‰ (from 10.10 to 16.84 ‰), and similarly to $\delta^{18}O$, showed no clear gradient with elevation or longitude. Deuterium excess showed a significant correlation with latitude, at $\rho = 0.60$ ($p < 0.01$). A more detailed analysis of d by latitude showed that only significantly different values were obtained in snow pits sampled beyond 79.2 °N, i.e., in Austfonna snow pits.. This is confirmed by the Kruskal-Wallis test, i.e. rank-based ANOVA, calculated with two groups of d values divided by the latitude threshold 79.2°N; $z = 4.23$, $p < 0.04$; in fact, drawing the latitude threshold anywhere between 78.7 and 79.7 °N resulted in a statistically significant difference with $p < 0.05$). This is consistent with lower temperatures and evaporation rates in

476 the more northern waters around Svalbard, and suggests that snowfall on AF is at least partly affected by
477 a different, more northerly moisture source than the rest of the archipelago.
478 ***4.5 Effect of elevation: a case study of Na***
479 The glacier survey carried out during the C2S3 project afforded the opportunity to investigate the
480 possible effect of elevation on the ionic composition of the snowpack. To do this, we compared the bulk
481 load and SWE-weighted mean concentration of Na^+ across all studied snowpits, ordered by elevation
482 (Figure 6). Overall, both Na^+ load and concentration decreased with increasing altitude (ρ_{load} = -0.24, not
483 significant; ρ_{conc} = -0.72, $p < 0.05$). This likely reflects greater local sea spray aerosol deposition at lower,
484 compared to higher glacier sites. We then computed linear (Pearson) correlation coefficients (*R*, with
485 associated *p*-values) between log-transformed Na^+ loading ($\log(Na_{load})$) and $\delta^{18}O$ for all snowpits in the
486 accumulation zones of glaciers (Figure 7). The calculation was performed with all snow layers. The Na^+
487 load was used as sea-spray tracer, while the $\delta^{18}O$ was assumed to vary with moisture source between
488 discrete snowfall events. We found that the positive correlation between $\log(Na_{load})$ and $\delta^{18}O$ increased
489 with elevation from R = 0.1 (HB3; 396 m a.s.l.) to R = 0.65 (LF3; 1193 m a.s.l.), and reached a 95 %
490 threshold of significance ($R > 0.3$) for glacier sites above 600 m a.sl. (KVG, AF, LF and HDF; Figure 7).
491 The average distance from the sea was a comparatively negligible factor in explaining the correlation
492 between $\log(Na_{load})$ and $\delta^{18}O$.
493
494 The increase in strength and significance of the $\log(Na_{load})$-$\delta^{18}O$ correlation with altitude might be
495 explained by different contributions of locally emitted $ssNa^+$, relative to those of Na^+ from more distant
496 sources. Sites located at lower altitudes are proportionally more affected by local sea spray deposition,
497 with or without snowfall. Conversely, sites at higher elevations likely receive a larger share of their ionic
498 load from more distant sources, and by wet deposition through snowfall. At the four sites (KVG, AF, LF,
499 and HDF) where the $\log(Na_{load})$-$\delta^{18}O$ correlation was significant, increases in $\delta^{18}O$ in snow layers were
500 often associated with higher Na^+ concentrations. It is rather difficult to propose a precise explanation for
501 this association. However, we would suggest that the isotopically heavier (less negative) $\delta^{18}O$ values
502 suggest that the co-registered Na^+ enhancements were associated with precipitation of relatively warm
503 air, probably advected from lower latitudes. The snowfall associated with a warm event is able to wet
504 scavenge the sea spray aerosol present in the atmosphere. On the contrary, when the cold air masses
505 (Arctic type) dominated, the snowfall events were relatively limited due to the poor air humidity causing
506 a lower efficiency of wet scavenging. This resulted in lower $\delta^{18}O$ and (likely) Na sodium loads,
507 suggesting that wet deposition dominated the chemical load of the snowpack. Although this process is
508 should occur also at lower elevation sites, the local emission and associated dry deposition are likely
509 more important than wet deposition; more frequent melt-refreeze episodes at lower elevations would also
510 mask the relationship proposed (as suggested by the vertical profiles of stratigraphy reported in Figure
511 S4).

Another possible explanation is that in the Arctic, air masses are transported from low to high elevation sites without any strong disturbance of the atmospheric conditions. In this case, isotopically heavier molecules and sea spray particles are gradually scavenged from the air masses. If this was the main process, we should find the correlation across all studied sites, assuming that Na^+ scavenged at a similar rate as that of isotopic fractionation. Since this has not been found, we propose that the correlation at higher elevation cannot be explained by atmospheric distillation alone. The possibility that the correlation is due to different sources of air masses seems unsupported due to the absence of correlation between d-excess and sodium.

5. Summary and Conclusion

We have quantified and described, for the first time, the spatial distribution of major ion loads (Ca^{2+}, K^+, Na^{2+}, Mg^{2+}, NH_4^+, SO_4^{2-}, Br^-, Cl^- and NO_3^-) and variations of $\delta^{18}O$ and δ^2H in the snowpack on glaciers across Svalbard for a single accumulation season (2015-2016). The highest total ionic loads were found in the southern region of Spitsbergen (Hornsund area), and exceeded 8 g m^{-2}. Conversely, the lowest total ionic loads ($\leq$ 0.6 g m^{-2}) were found at sites in central or northwestern Spitsbergen (LF and HDF). Sea salt ions (Cl^-, Na^+, and SO_4^{2-}) dominated the ionic loads at all sites, but their share was highest at sites near Hornsund, for, e.g., 48% Cl^-, compared to only 29% on Holtedahlfonna. Relatively elevated Ca^{2+}/Mg^{2+} ratios in snow at all sites indicated non-sea-salt Ca^{2+} inputs, most likely in the form of carbonate dust. Unlike other ions, NO_3^- had the highest loads in glaciers of northwestern Spitsbergen, and the lowest at LF. The nitrogen species, NO_3^- and NH_4^+, showed distinct spatial distribution patterns. The highest NO_3^- loads were found in the northwestern part of Svalbard, while the highest NH_4^+ loads were in the southwest. Bromide (Br^-) was most enriched in snow relative to seawater at AF and LF, the glacier sites located closest to areas with first-year sea ice cover. This supports first-year sea ice being an important source of non-sea salt Br^- in the polar atmosphere.

An increasing positive correlation between $\log(Na_{load})$ and $\delta^{18}O$ as a function of elevation sites suggests that locations above 600-700 m a.s.l. are influenced by a proportionally higher share of ions from distant sources, while the lower sites are exposed to more local sources, especially sea spray. These findings confirm that the optimal sites to study the effects of long-range pollution deposition in Svalbard are those found at higher elevation sites, such as the accumulation zones of HDF or LF, because they are the least impacted by the local aerosol emissions. The current study gives the first picture of the ionic composition in the Svalbard snowpack in different regions across the archipelago, in the context of which processes are relevant in controlling the annual snowpack chemical composition there, especially the influence of local and long-range transport.

Acknowledgements

549 The work developed here was supported through grants 246731/E10 and 257636/E10 from the Svalbard
550 Science Forum /Research Council of Norway, by the Gothenburg Centre of Advanced Studies, BECC -
551 Biodiversity and Ecosystem Services in a Changing Climate, Gothenburg Air and Climate Centre,
552 International Arctic Science Committee - Cryosphere working group and the Norwegian Polar Institute.
553 Part of fieldwork has been conducted thanks to the funds of the Leading National Research Centre
554 (KNOW) in Poland, received by the Centre for Polar Studies for the period 2014–2018. This research
555 was also partially supported within statutory activities No 3841/E-41/S/2020 of the Ministry of Science
556 and Higher Education of Poland. The project has received further funding from the European Union's
557 Horizon 2020 research and innovation programme under grant agreement no. 689443 via project iCUPE
558 (Integrative and Comprehensive Understanding on Polar Environments).
559

560 **Author Contribution**

561 EB, KK and AS wrote the manuscript, with contributions from all co-authors. JCG, MB, CL, BL, TS,
562 CZ, FL, DK, AS, EB, TM, KK and AU initiated the April 2016 survey. EB, KK CPV and CZ perform
563 the analytical measurements, TM the δ18O analyses.
564
565

REFERENCES

Aas, K. S., Dunse, T., Collier, E., Schuler, T. V., Berntsen, T. K., Kohler, J., and Luks, B.: The climatic mass balance of Svalbard glaciers: a 10-year simulation with a coupled atmosphere–glacier mass balance model, The Cryosphere, 10, 1089-1104, 2016.

Ardyna, M., Babin, M., Gosselin, M., Devred, E., Bélanger, S., Matsuoka, A., and Tremblay, J.-E.: Parameterization of vertical chlorophyll a in the Arctic Ocean: impact of the subsurface chlorophyll maximum on regional, seasonal, and annual primary production estimates, Biogeosciences, 10, 4383–4404, 2013.

Barbante, C., Spolaor, A., Cairns, W. R. L., and Boutron, C.: Man's footprint on the Arctic environment as revealed by analysis of ice and snow, Earth-Sci Rev, 168, 218-231, 2017.

Barbaro, E., Padoan, S., Kirchgeorg, T., Zangrando, R., Toscano, G., Barbante, C., and Gambaro, A.: Particle size distribution of inorganic and organic ions in coastal and inland Antarctic aerosol, Environmental Science and Pollution Research, 24, 2724-2733, 2017.

Barrie, L. A.: Arctic air pollution: An overview of current knowledge, Atmospheric Environment (1967), 20, 643-663, 1986.

Beaudon, E., Moore, J. C., Martma, T., Pohjola, V. A., Van de Wal, R. S. W., Kohler, J., and Isaksson, E.: Lomonosovfonna and Holtedahlfonna ice cores reveal east–west disparities of the Spitsbergen environment since AD 1700, J Glaciol, 59, 1069-1083, 2017.

Björkman, M. P., Vega, C. P., Kühnel, R., Spataro, F., Ianniello, A., Esposito, G., Kaiser, J., Marca, A., Hodson, A., Isaksson, E., and Roberts, T. J.: Nitrate postdeposition processes in Svalbard surface snow, Journal of Geophysical Research: Atmospheres, 119, 12,953-912,976, 2014.

Brage, B. H., Ketil Isaksen, Rasmus E. Benestad, Jack Kohler, Åshild Ø Pedersen, Leif E Loe, Stephen J. Coulson, Jan Otto Larsen, and Varpe., Ø.: Warmer and wetter winters: characteristics and implications of an extreme weather event in the High Arctic, Environ. Res. Lett., 9, 2014.

Brimblecombe, P., Clegg, S. L., Davies, T. D., Shooter, D., and Tranter, M.: Observations of the preferential loss of major ions from melting snow and laboratory ice, Water Research, 21, 1279-1286, 1987.

Cogley, J. G., R. Hock, L.A. Rasmussen, A.A. Arendt, A. Bauder, R.J. Braithwaite, P. Jansson, G. Kaser, M. Möller, Nicholson, L., and Zemp., M.: Glossary of Glacier Mass Balance and Related Terms, IHP-VII Technical Documents in Hydrology, IACS Contribution No. 2, Unesco-IHP, Paris, 86, 2011.

Curtis, C. J., Kaiser, J., Marca, A., Anderson, N. J., Simpson, G., Jones, V., and Whiteford, E.: Spatial variations in snowpack chemistry, isotopic composition of NO3− and nitrogen deposition from the ice sheet margin to the coast of western Greenland, Biogeosciences, 15, 529-550, 2018.

Dahlke, S., Hughes, N. E., Wagner, P. M., Gerland, S., Wawrzyniak, T., Ivanov, B., and Maturilli, M.: The observed recent surface air temperature development across Svalbard and concurring footprints in local sea ice cover, International Journal of Climatology, n/a, 2020.

Dallmann, W. K.: The geology of Svalbard, Norwegian Polar Institute, 1999.

Dallmann, W. K.: Geoscience Atlas of Svalbard, Norsk polarinstitutt Rapportserie, 2015.

Eneroth, K., Kjellström, E., and Holmén, K.: A trajectory climatology for Svalbard; investigating how atmospheric flow patterns influence observed tracer concentrations, Physics and Chemistry of the Earth, Parts A/B/C, 28, 1191-1203, 2003.

Fibiger, D. L., Dibb, J. E., Chen, D., Thomas, J. L., Burkhart, J. F., Huey, L. G., and Hastings, M. G.: Analysis of nitrate in the snow and atmosphere at Summit, Greenland: Chemistry and transport, Journal of Geophysical Research: Atmospheres, 121, 5010-5030, 2016.

Forland, E. J., Benestad, R., Hanssen-Bauer, I., Haugen, J. E., and Skaugen, T. E.: Temperature and Precipitation Development at Svalbard 1900–2100, Advances in Meteorology, 2011, 14, 2011.

Forsström, S., Ström, J., Pedersen, C. A., Isaksson, E., and Gerland, S.: Elemental carbon distribution in Svalbard snow, Journal of Geophysical Research: Atmospheres, 114, 2009.

Gallet, J. C., Bjorkman, M. P., Larose, C., Luks, B., Martma, T., and Zdanowicz, C.: Protocols and recommendations for the measurement of snow physical properties, and sampling of snow for black carbon, water isotopes, major ions and microorganisms, Norsk Polarinstitutt, 46, 2018.

Gat, J. R.: OXYGEN AND HYDROGEN ISOTOPES IN THE HYDROLOGIC CYCLE, Annual Review of Earth and Planetary Sciences, 24, 225-262, 1996.
Gat, J. R., Mook, W. G., and H.A.J., M.: Atmospheric Water. In: Environmental Isotopes in the Hydrological Cycle, Principle and Applications, International Atomic Energy Agency, Vienna, 2001.
Gibson, E. R., Hudson, P. K., and Grassian, V. H.: Physicochemical Properties of Nitrate Aerosols: Implications for the Atmosphere, The Journal of Physical Chemistry A, 110, 11785-11799, 2006.
Gondwe, M., Krol, M., Gieskes, W., Klaassen, W., and de Baar, H.: The contribution of ocean-leaving DMS to the global atmospheric burdens of DMS, MSA, SO2, and NSS SO4=, Global Biogeochem Cy, 17, 2003.
Hodgkins, R. and Tranter, M.: Solute in high arctic glacier snow cover and its impact on runoff chemistry, Annals of Glaciology, 26, 156-160, 1998.
Igarashi, M., Kamiyama, K., and Watanabe, O.: Stable oxygen isotope ratio observed in the precipitation at Ny-Alesund, Svalbard, Mem. Natl Inst. Polar Res., Spec. Issue, 54, 69-182, 2001.
Isaksen, K., Nordli, Ø., Førland, E. J., Łupikasza, E., Eastwood, S., and Niedźwiedź, T.: Recent warming on Spitsbergen—Influence of atmospheric circulation and sea ice cover, Journal of Geophysical Research: Atmospheres, 121, 11,913-911,931, 2016.
Isaksson, E., Hermanson, M., Hicks, S., Igarashi, M., Kamiyama K, Moore, J., Motoyama, H., Muir, D., Pohjola, V., Vaikmae, R., Van de Wal, R. S. W., and Watanabe, O.: Ice cores from Svalbard—useful archives of past climate and pollution history, 28, 1217-1228, 2003.
Isaksson, E., Pohjola, V., Jauhiainen, T., Moore, J., Pinglot, J. F., Vaikmäe, R., van De Wal, R. S. W., Hagen, J. O., Ivask, J., Karlöf, L., Martma, T., Meijer, H. A. J., Mulvaney, R., Thomassen, M., and van den Broeke, M.: A new ice-core record from Lomonosovfonna, Svalbard: viewing the 1920–97 data in relation to present climate and environmental conditions, J Glaciol, 47, 335-345, 2001.
Jacobi, H. W., Obleitner, F., Da Costa, S., Ginot, P., Eleftheriadis, K., Aas, W., and Zanatta, M.: Deposition of ionic species and black carbon to the Arctic snowpack: combining snow pit observations with modeling, Atmos. Chem. Phys., 19, 10361-10377, 2019.
Jason B. West, Gabriel J. Bowen, Todd E. Dawson, and Tu., K. P.: Understanding movement, pattern, and process on Earth through isotope mapping, Springer Netherlands, 2010.
Johnsen, S. J., Dansgaard, W., and White, J. W. C.: The origin of Arctic precipitation under present and glacial conditions, Tellus B: Chemical and Physical Meteorology, 41, 452-468, 1989.
Karl, M., Leck, C., Mashayekhy Rad, F., Bäcklund, A., Lopez-Aparicio, S., and Heintzenberg, J.: New insights in sources of the sub-micrometre aerosol at Mt. Zeppelin observatory (Spitsbergen) in the year 2015, Tellus B: Chemical and Physical Meteorology, 71, 1613143, 2019.
Kekonen, T., Moore, J., Perämäki, P., Mulvaney, R., Isaksson, E., Pohjola, V., and van de Wal, R. S. W.: The 800 year long ion record from the Lomonosovfonna (Svalbard) ice core, Journal of Geophysical Research: Atmospheres, 110, 2005.
Kekonen, T., Moore, J. C., Mulvaney, R., Isaksson, E., Pohjola, V., and van de Wal, R. S. W.: A 800 year record of nitrate from the Lomonosovfonna ice core, Svalbard, Annals of Glaciology, 35, 261-265, 2017.
Keslinka, L. K., Wojczulanis-Jakubas, K., Jakubas, D., and Neubauer, G.: Determinants of the little auk (Alle alle) breeding colony location and size in W and NW coast of Spitsbergen, PLOS ONE, 14, e0212668, 2019.
Kuhn, M.: The nutrient cycle through snow and ice, a review, Aquatic Sciences, 63, 150-167, 2001.
Kühnel, R., Roberts, T. J., Björkman, M. P., Isaksson, E., Aas, W., Holmén, K., and Ström, J.: 20-Year Climatology of NO3 and NH4+ Wet Deposition at Ny-Alesund, Svalbard, Advances in Meteorology, 2011, 10, 2011.
Law, K. S. and Stohl, A.: Arctic Air Pollution: Origins and Impacts, Science, 315, 1537, 2007.
Lindbäck, K., Kohler, J., Pettersson, R., Nuth, C., Langley, K., Messerli, A., Vallot, D., Matsuoka, K., and Brandt, O.: Subglacial topography, ice thickness, and bathymetry of Kongsfjorden, northwestern Svalbard, Earth Syst. Sci. Data, 10, 1769-1781, 2018.
Marlin, C., Tolle, F., Griselin, M., Bernard, E., Saintenoy, A., Quenet, M., and Friedt, J.-M.: Change in geometry of a high Arctic glacier from 1948 to 2013 (Austre Lovénbreen, Svalbard), Geografiska Annaler: Series A, Physical Geography, 99, 115-138, 2017.

673 Matoba, S., Narita, H., Motoyama, H., Kamiyama, K., and Watanabe, O.: Ice core chemistry of
674 Vestfonna Ice Cap in Svalbard, Norway, Journal of Geophysical Research: Atmospheres, 107, ACH
675 19-11-ACH 19-17, 2002.
676 Maturilli, M., Herber, A., and König-Langlo, G.: Climatology and time series of surface meteorology in
677 Ny-Älesund, Svalbard, Earth Syst. Sci. Data, 5, 155-163, 2013.
678 Melvold, K. Hagen, J.O. Evolution of a surge-type glacier in its quiescent phase: Kongsvegen,
679 Spitsbergen, 1964-95. Journal of Glaciology, Vo!. 44, No. 147, 199
680 Millero, F. J., Feistel, R., Wright, D. G., and McDougall, T. J.: The composition of Standard Seawater
681 and the definition of the Reference-Composition Salinity Scale, Deep Sea Research Part I:
682 Oceanographic Research Papers, 55, 50-72, 2008.
683 Möller, M. and Kohler, J.: Differing Climatic Mass Balance Evolution Across Svalbard Glacier Regions
684 Over 1900–2010, Frontiers in Earth Science, 6, 128, 2018.
685 Nawrot, A. P., Migała, K., Luks, B., Pakszys, P., and Głowacki, P.: Chemistry of snow cover and acidic
686 snowfall during a season with a high level of air pollution on the Hans Glacier, Spitsbergen, Polar
687 Science, 10, 249-261, 2016.
688 Nordli, Ø., Przybylak, R., Ogilvie, A. E. J., and Isaksen, K.: Long-term temperature trends and
689 variability on Spitsbergen: the extended Svalbard Airport temperature series, 1898–2012, Polar Res,
690 33, 21349, 2014.
691 Nuth, C., Schuler, T. V., Kohler, J., Altena, B., and Hagen, J. O.: Estimating the long-term calving flux
692 of Kronebreen, Svalbard, from geodetic elevation changes and mass-balance modeling, J Glaciol, 58,
693 119-133, 2017.
694 Peterson, P. K., Hartwig, M., May, N. W., Schwartz, E., Rigor, I., Ermold, W., Steele, M., Morison, J.
695 H., Nghiem, S. V., and and Pratt, K. A.: Snowpack measurements suggest role for multi-year sea ice
696 regions in Arctic atmospheric bromine and chlorine chemistry, Elem Sci Anth, 7(1), 14, 2019.
697 Pohjola, V. A., Martma, T. A., Meijer, H. A. J., Moore, J. C., Isaksson, E., Vaikmäe, R., and van de Wal,
698 R. S. W.: Reconstruction of three centuries of annual accumulation rates based on the record of stable
699 isotopes of water from Lomonosovfonna, Svalbard, Annals of Glaciology, 35, 57-62, 2017.
700 Pohjola, V. A., Moore, J. C., Isaksson, E., Jauhiainen, T., van de Wal, R. S. W., Martma, T., Meijer, H.
701 A. J., and Vaikmäe, R.: Effect of periodic melting on geochemical and isotopic signals in an ice core
702 from Lomonosovfonna, Svalbard, Journal of Geophysical Research: Atmospheres, 107, ACL 1-1-
703 ACL 1-14, 2002.
704 Punning, Y. M. K., Martma, T. A., Tyugu, K. E., Vaykmyae, R. A., Purshe, M., and Pinglo, F.:
705 Stratification in an Ice core from Vestfonna, Nordaustlandet, Polar Geography and Geology, 10, 39-
706 43, 1986.
707 Rinke, A., Maturilli, M., Graham, R. M., Matthes, H., Handorf, D., Cohen, L., Hudson, S. R., and
708 Moore, J. C.: Extreme cyclone events in the Arctic: Wintertime variability and trends, Environ Res
709 Lett, 12, 094006, 2017.
710 Schaap, M., van Loon, M., ten Brink, H. M., Dentener, F. J., and Builtjes, P. J. H.: Secondary inorganic
711 aerosol simulations for Europe with special attention to nitrate, Atmos. Chem. Phys., 4, 857-874,
712 2004.
713 Schuler, T. V., Glazovsky, A., Hagen, J. O., Hodson, A., Jania, J., Kääb, A., Kohler, J., Luks, B.,
714 Malecki, J., Moholdt, G., Pohjola, V., and Pelt, W. V.: New data, new techniques and new challenges
715 for updating the state of Svalbard glaciers (SvalGlac), Longyearbyen, 108-134 pp., 2020.
716 Schüpbach, S., Fischer, H., Bigler, M., Erhardt, T., Gfeller, G., Leuenberger, D., Mini, O., Mulvaney, R.,
717 Abram, N. J., Fleet, L., Frey, M. M., Thomas, E., Svensson, A., Dahl-Jensen, D., Kettner, E., Kjaer,
718 H., Seierstad, I., Steffensen, J. P., Rasmussen, S. O., Vallelonga, P., Winstrup, M., Wegner, A.,
719 Twarloh, B., Wolff, K., Schmidt, K., Goto-Azuma, K., Kuramoto, T., Hirabayashi, M., Uetake, J.,
720 Zheng, J., Bourgeois, J., Fisher, D., Zhiheng, D., Xiao, C., Legrand, M., Spolaor, A., Gabrieli, J.,
721 Barbante, C., Kang, J. H., Hur, S. D., Hong, S. B., Hwang, H. J., Hong, S., Hansson, M., Iizuka, Y.,
722 Oyabu, I., Muscheler, R., Adolphi, F., Maselli, O., McConnell, J., and Wolff, E. W.: Greenland
723 records of aerosol source and atmospheric lifetime changes from the Eemian to the Holocene, Nature
724 Communications, 9, 1476, 2018.
725 Semb, A., Brækkan, R., and Joranger, E.: Major ions in Spitsbergen snow samples, Geophys Res Lett,
726 11, 445-448, 1984.

727 Spolaor, A., Barbaro, E., Cappelletti, D., Turetta, C., Mazzola, M., Giardi, F., Björkman, M. P.,
728 Lucchetta, F., Dallo, F., Pfaffhuber, K. A., Angot, H., Dommergue, A., Maturilli, M., Saiz-Lopez, A.,
729 Barbante, C., and Cairns, W. R. L.: Diurnal cycle of iodine, bromine, and mercury concentrations in
730 Svalbard surface snow, Atmos. Chem. Phys., 19, 13325-13339, 2019.
731 Spolaor, A., Barbaro, E., Christille, J. M., Kirchgeorg, T., Giardi, F., Cappelletti, D., Turetta, C.,
732 Bernagozzi, A., Björkman, M. P., Bertolini, E., and Barbante, C.: Evolution of the Svalbard annual
733 snow layer during the melting phase, Rendiconti Lincei, doi: 10.1007/s12210-015-0500-8, 2016. 1-8,
734 2016.
735 Spolaor, A., Barbaro, E., Mazzola, M., Viola, A. P., Lisok, J., Obleitner, F., Markowicz, K. M., and
736 Cappelletti, D.: Determination of black carbon and nanoparticles along glaciers in the Spitsbergen
737 (Svalbard) region exploiting a mobile platform, Atmos Environ, 170, 184-196, 2017.
738 Spolaor, A., Gabrieli, J., Martma, T., Kohler, J., Björkman, M. B., Isaksson, E., Varin, C., Vallelonga,
739 P., Plane, J. M. C., and Barbante, C.: Sea ice dynamics influence halogen deposition to Svalbard, The
740 Cryosphere, 7, 1645-1658, 2013.
741 Spolaor, A., Vallelonga, P., Gabrieli, J., Martma, T., Björkman, M. P., Isaksson, E., Cozzi, G., Turetta,
742 C., Kjær, H. A., Curran, M. A. J., Moy, A. D., Schönhardt, A., Blechschmidt, A. M., Burrows, J. P.,
743 Plane, J. M. C., and Barbante, C.: Seasonality of halogen deposition in polar snow and ice, Atmos.
744 Chem. Phys., 14, 9613-9622, 2014.
745 Thompson, L. G., Mosley-Thompson, E., Davis, M. E., Henderson, K. A., Brecher, H. H., Zagorodnov,
746 V. S., Mashiotta, T. A., Lin, P.-N., Mikhalenko, V. N., Hardy, D. R., and Beer, J. r.: Kilimanjaro Ice
747 Core Records: Evidence of Holocene Climate Change in Tropical Africa, Science, 298, 589-593,
748 2002.
749 Trachsel, J. C., Avak, S. E., Edebeli, J., Schneebeli, M., Bartels-Rausch, T., Bruetsch, S., and Eichler,
750 A.: Microscale Rearrangement of Ammonium Induced by Snow Metamorphism, Frontiers in Earth
751 Science, 7, 194, 2019.
752 Uemura, R., Matsui, Y., Yoshimura, K., Motoyama, H., and Yoshida, N.: Evidence of deuterium excess
753 in water vapor as an indicator of ocean surface conditions, Journal of Geophysical Research:
754 Atmospheres, 113, 2008.
755 van Pelt, W., Pohjola, V., Pettersson, R., Marchenko, S., Kohler, J., Luks, B., Hagen, J. O., Schuler, T.
756 V., Dunse, T., Noël, B., and Reijmer, C.: A long-term dataset of climatic mass balance, snow
757 conditions, and runoff in Svalbard (1957–2018), The Cryosphere, 13, 2259-2280, 2019.
758 Vecchiato, M., Barbaro, E., Spolaor, A., Burgay, F., Barbante, C., Piazza, R., and Gambaro, A.:
759 Fragrances and PAHs in snow and seawater of Ny-Ålesund (Svalbard): Local and long-range
760 contamination, Environmental Pollution, 242, 1740-1747, 2018.
761 Vega, C. P., Björkman, M. P., Pohjola, V. A., Isaksson, E., Pettersson, R., Martma, T., Marca, A., and
762 Kaiser, J.: Nitrate stable isotopes in snow and ice samples from four Svalbard sites, Polar Res, 34,
763 2015a.
764 Vega, C. P., Pohjola, V. A., Beaudon, E., Claremar, B., van Pelt, W. J. J., Pettersson, R., Isaksson, E.,
765 Martma, T., Schwikowski, M., and Bøggild, C. E.: A synthetic ice core approach to estimate ion
766 relocation in an ice field site experiencing periodical melt; a case study on Lomonosovfonna,
767 Svalbard, The Cryosphere Discuss., 9, 5053-5095, 2015b.
768 Vega, C. P., Pohjola, V. A., Beaudon, E., Claremar, B., van Pelt, W. J. J., Pettersson, R., Isaksson, E.,
769 Martma, T., Schwikowski, M., and Bøggild, C. E.: A synthetic ice core approach to estimate ion
770 relocation in an ice field site experiencing periodical melt: a case study on Lomonosovfonna,
771 Svalbard, The Cryosphere, 10, 961-976, 2016.
772 Virkkunen, K., Moore, J. C., Isaksson, E., Pohjola, V., Perämäki, P., Grinsted, A., and Kekonen, T.:
773 Warm summers and ion concentrations in snow: comparison of present day with Medieval Warm
774 Epoch from snow pits and an ice core from Lomonosovfonna, Svalbard, J Glaciol, 53, 623-634, 2007.
775 Whitlow, S., Mayewski, P. A., and Dibb, J. E.: A comparison of major chemical species seasonal
776 concentration and accumulation at the South Pole and summit, Greenland, Atmospheric Environment.
777 Part A. General Topics, 26, 2045-2054, 1992.
778 Winther, M., Christensen, J. H., Plejdrup, M. S., Ravn, E. S., Eriksson, Ó. F., and Kristensen, H. O.:
779 Emission inventories for ships in the arctic based on satellite sampled AIS data, Atmos Environ, 91,
780 1-14, 2014.

781 Wojczulanis K., Jakubas D., and Stempniewicz, L.: Avifauna of Hornsund area, SW Spitsbergen:present
782 state and recent changes, Polish Polar Research, 29, 187-197, 2008.
783 Wolff, E. W., Barbante, C., Becagli, S., Bigler, M., Boutron, C. F., Castellano, E., De Angelis, M.,
784 Federer, U., Fischer, H., and Fundel, F.: Changes in environment over the last 800,000 years from
785 chemical analysis of the EPICA Dome C ice core, Quaternary Sci Rev, 29, 285-295, 2010.
786 Zhuang, H., Chan, C. K., Fang, M., and Wexler, A. S.: Formation of nitrate and non-sea-salt sulfate on
787 coarse particles, Atmos Environ, 33, 4223-4233, 1999.
788
789

790 **FIGURES**

791

792 **Figure 1.** Total snowpack loads (mg m^{-2}) of major ions in 22 snowpits collected on glaciers during the C2S3
793 project. Seven glaciers were sampled in three snowpits in the lower ablation zone (1), near the equilibrium
794 line (2) and in the upper accumulation zone (3), except on KVG glacier where there was an extra snowpit
795 sampled within the ablation zone.
796 Abbreviations: KVG = Kongsvegen, HDF = Holtedahlfonna, AF= Austfonna, ALB = Austre Lovénbreen, LF =
797 Lomonosovfonna, HB = Hansbreen, WB = Werenskiöldbreen.

798

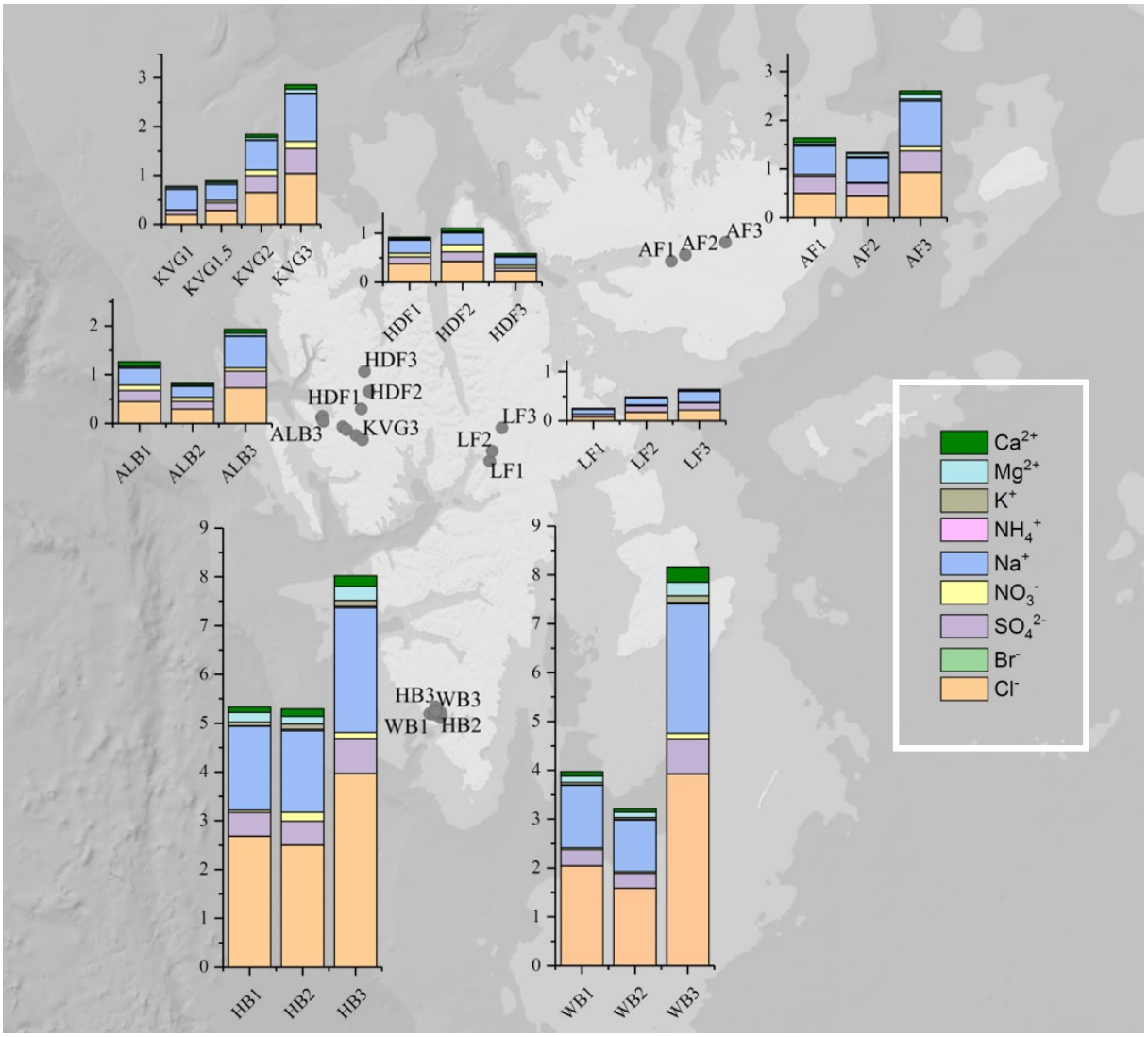

799

800

801

802

Figure 2. Calculated ionic loads in the snowpack (mg m^{-2}) at the 7 glacier sites sampled during the C2S3 project. Snowpits for each glacier are marked with the same colour and ordered from lower (left) to higher altitudes (right). For the KVG another snowpit was dug between glacier zones 1 and 2.

Abbreviation: KVG = Kongsvegen, HDF = Holtedahlfonna, AF= Austfonna, ALB = Austre Lovénbreen, LF = Lomonosovfonna, HB = Hansbreen, WB = Werenskiöldbreen.

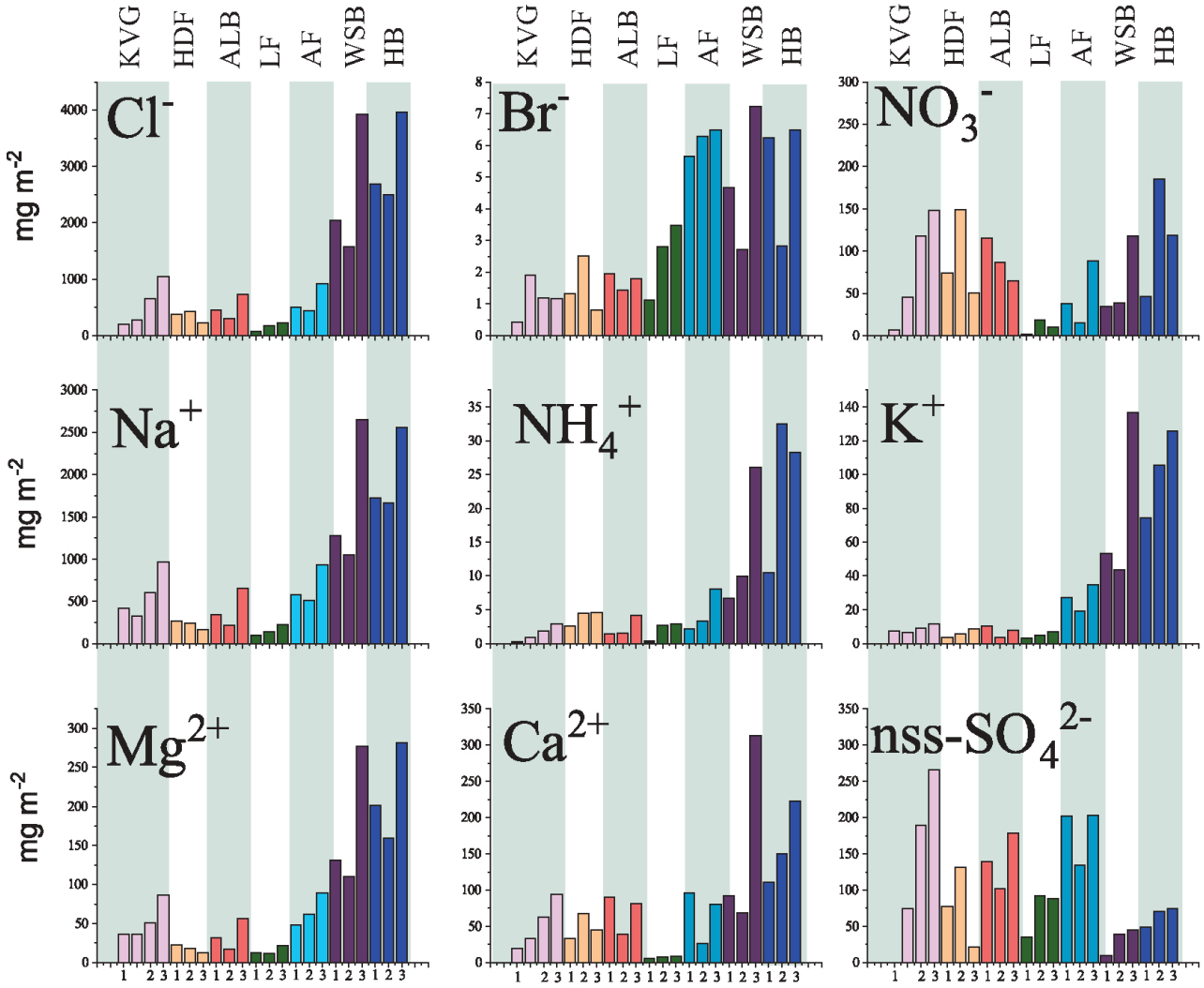

Figure 3. Pie diagrams showing relative ionic composition in the snowpits dug in the accumulation zones of the studied glaciers

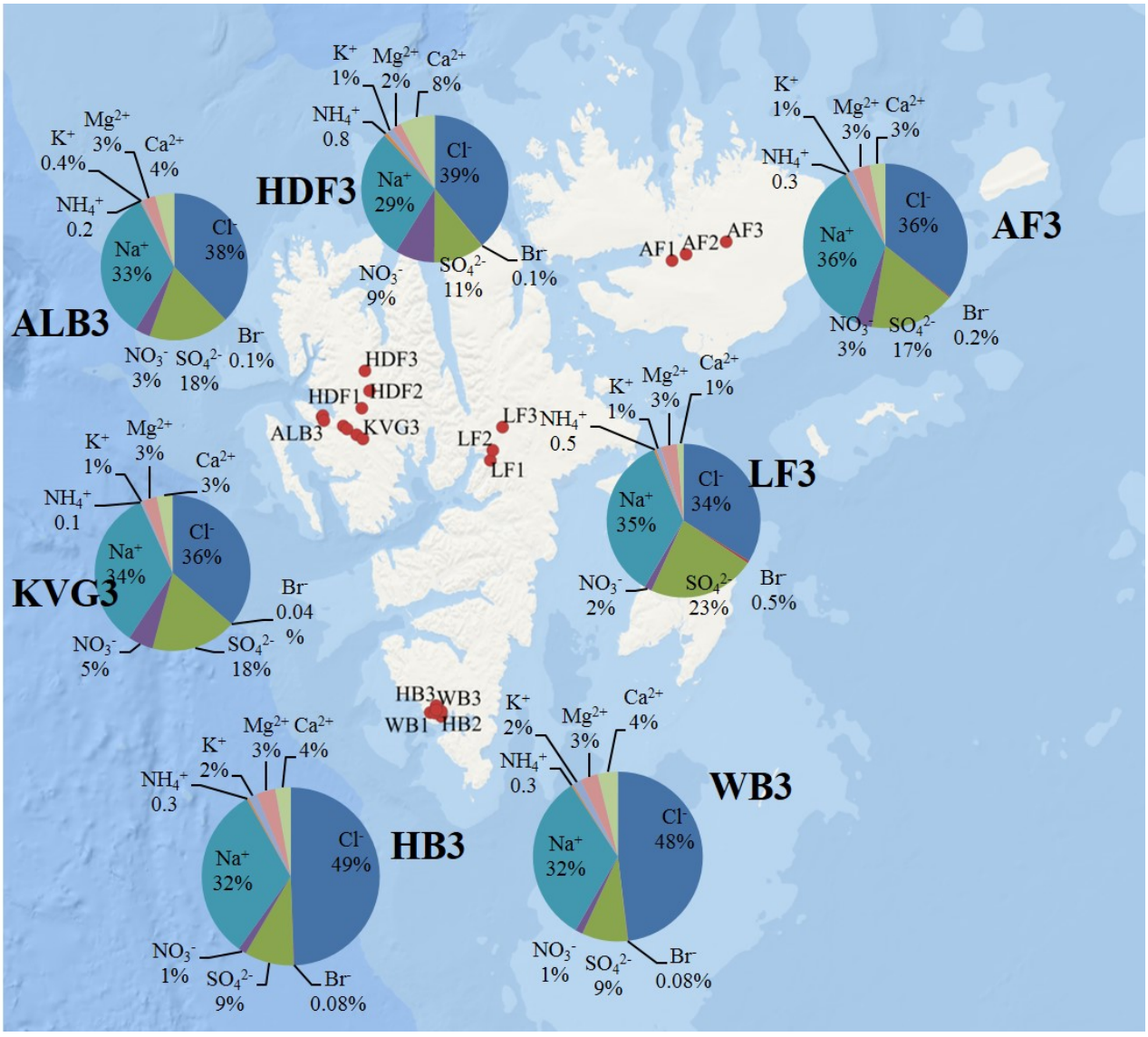

824 **Figure 4**. Box plots of stable water isotopes ($\delta^{18}O$ and $\delta^{2}H$) and deuterium excess (*d*) for each
825 snowpit.
826

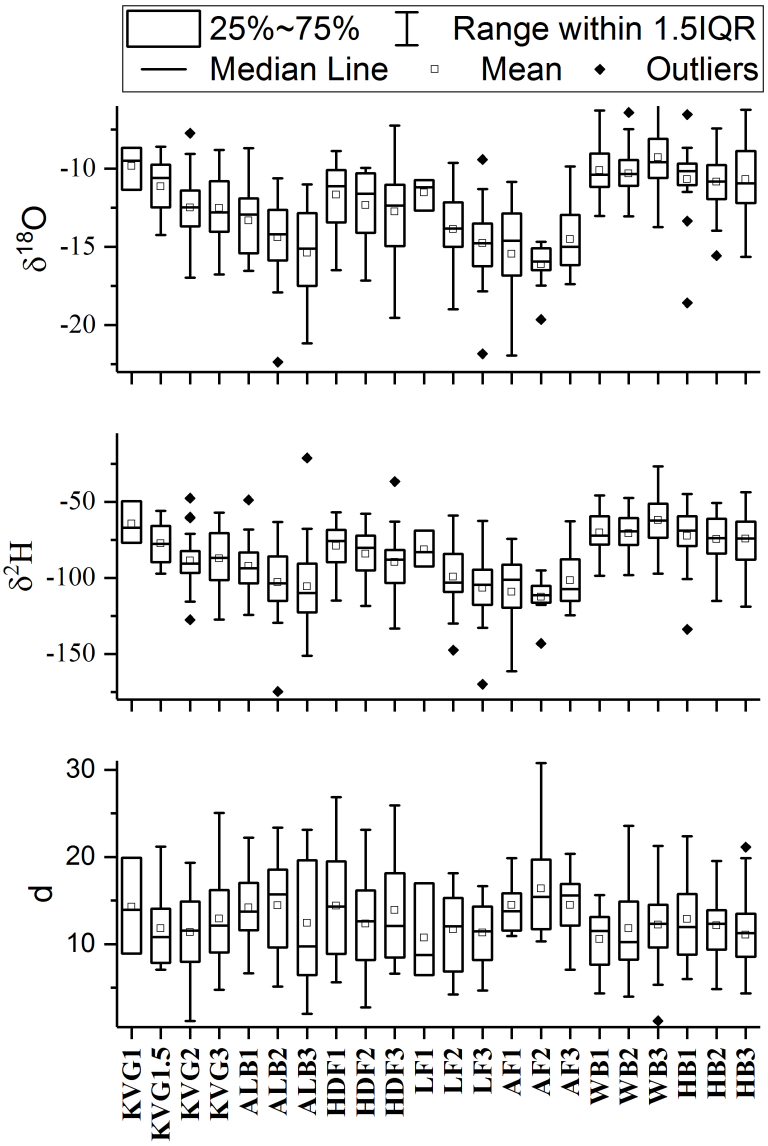

827
828
829
830
831
832
833

Figure 5. Panels from top: 1) Cl^-/Na^+; 2) Na^+/SO_4^{2-}; 3) Cl^-/SO_4^{2-}; 4) the total loads of sea-salt sulphate (ss-SO_4^{2-}) and non-sea-salt sulphate (nss-SO_4^{2-}), and 5) Ca^{2+}/Mg^{2+} for all glaciers investigated during the C2S3 project (in spring 2016).

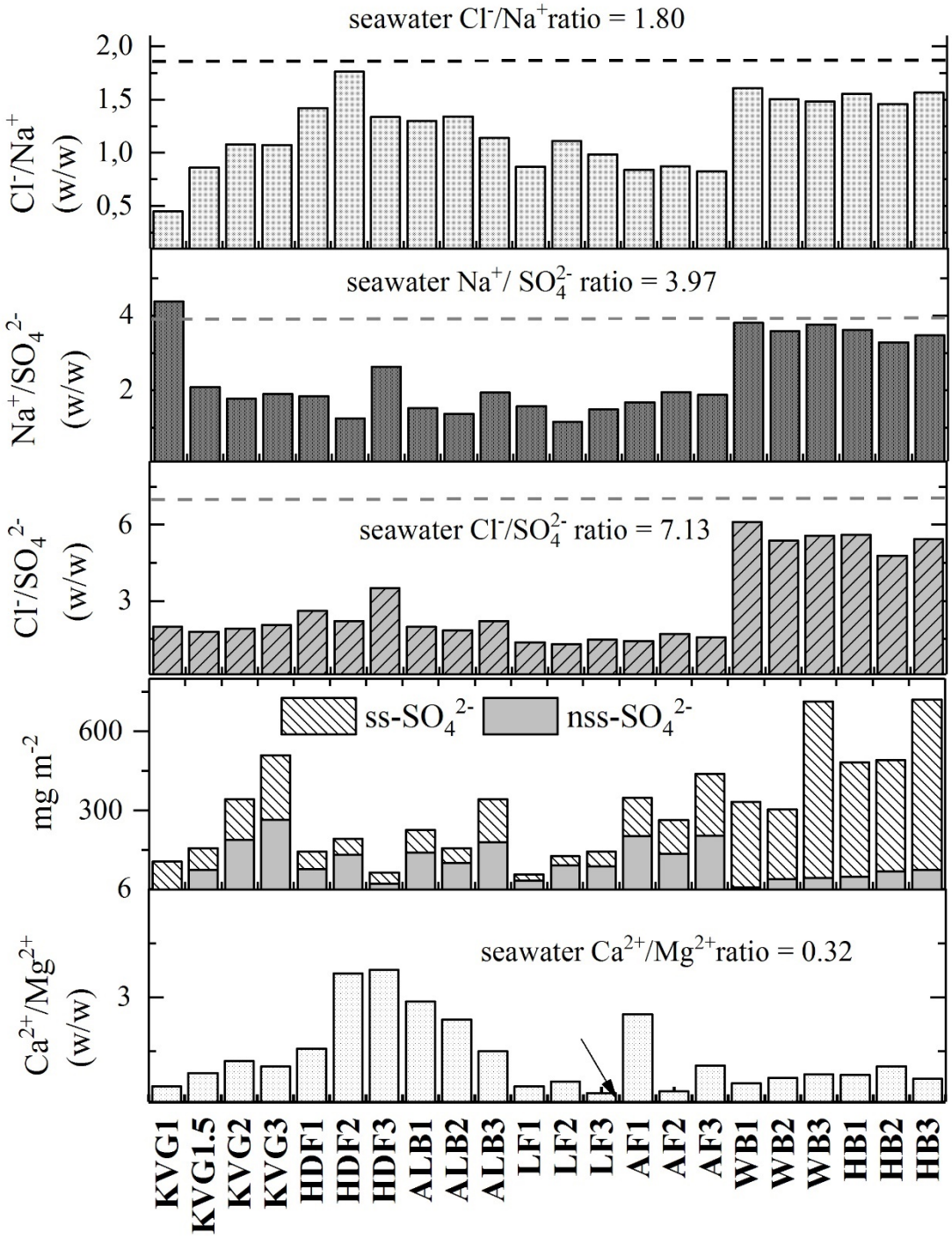

Figure 6. Sodium load in snowpits ordered by increasing elevation in m a.s.l., indicated by the red lines. The colours identify areas where the snowpits have been excavated: each colour represents a separate glacier (HB – blue; WB – purple; ALB – red; LF – green; KVG – pink; AF – light blue; HDF – orange). IQR = inter-quartile range, i.e. the difference between the value of quartiles 3 and 1.

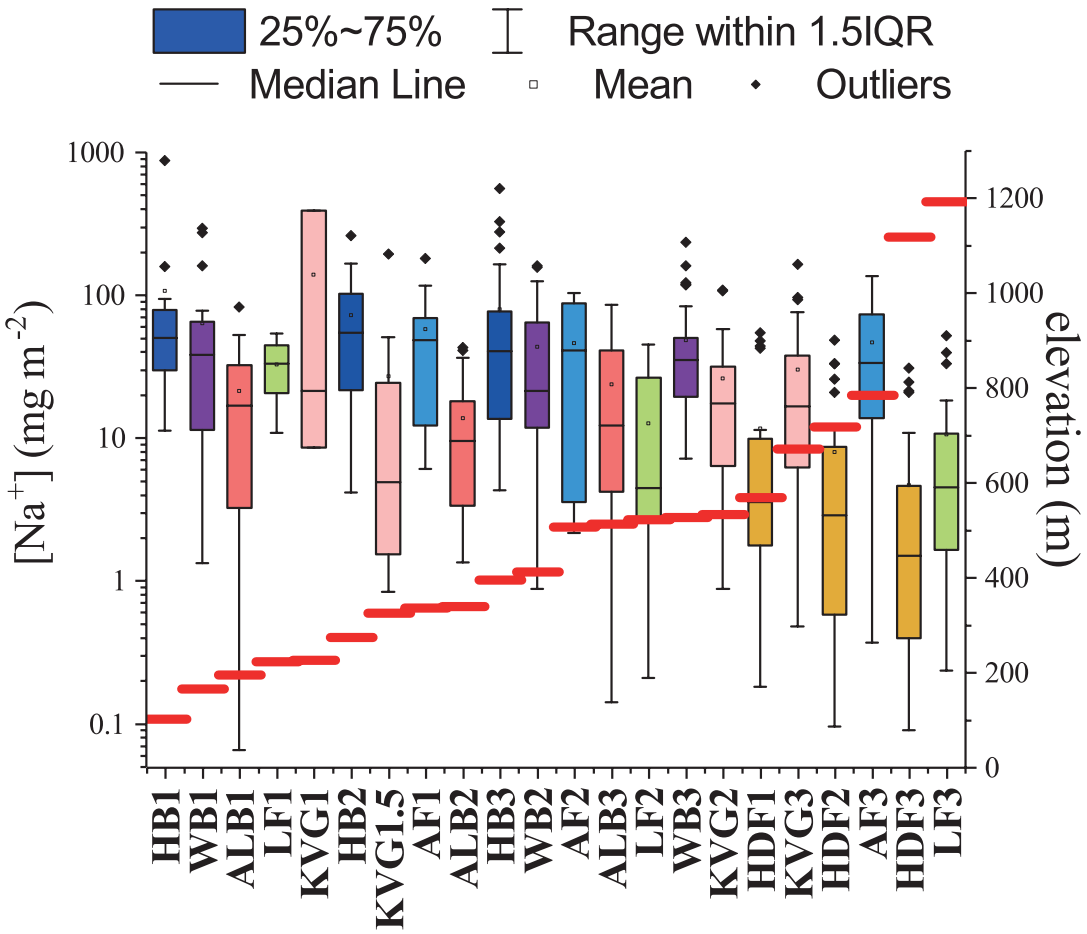

Figure 7. The correlation coefficient between the oxygen isotope ratio ($\delta^{18}O$) and log[Na_{load}] increases with elevation. The left axis represents the correlation coefficient (R) between log[Na_{load}] and $\delta^{18}O$, using the entire dataset for each snowpit (i.e. all layers have been used for the statistical correlation). The *x axis* indicates the altitude of the snowpit. The upper panel shows the p-value: correlations have been considered statistically significant if $p < 0.05$.

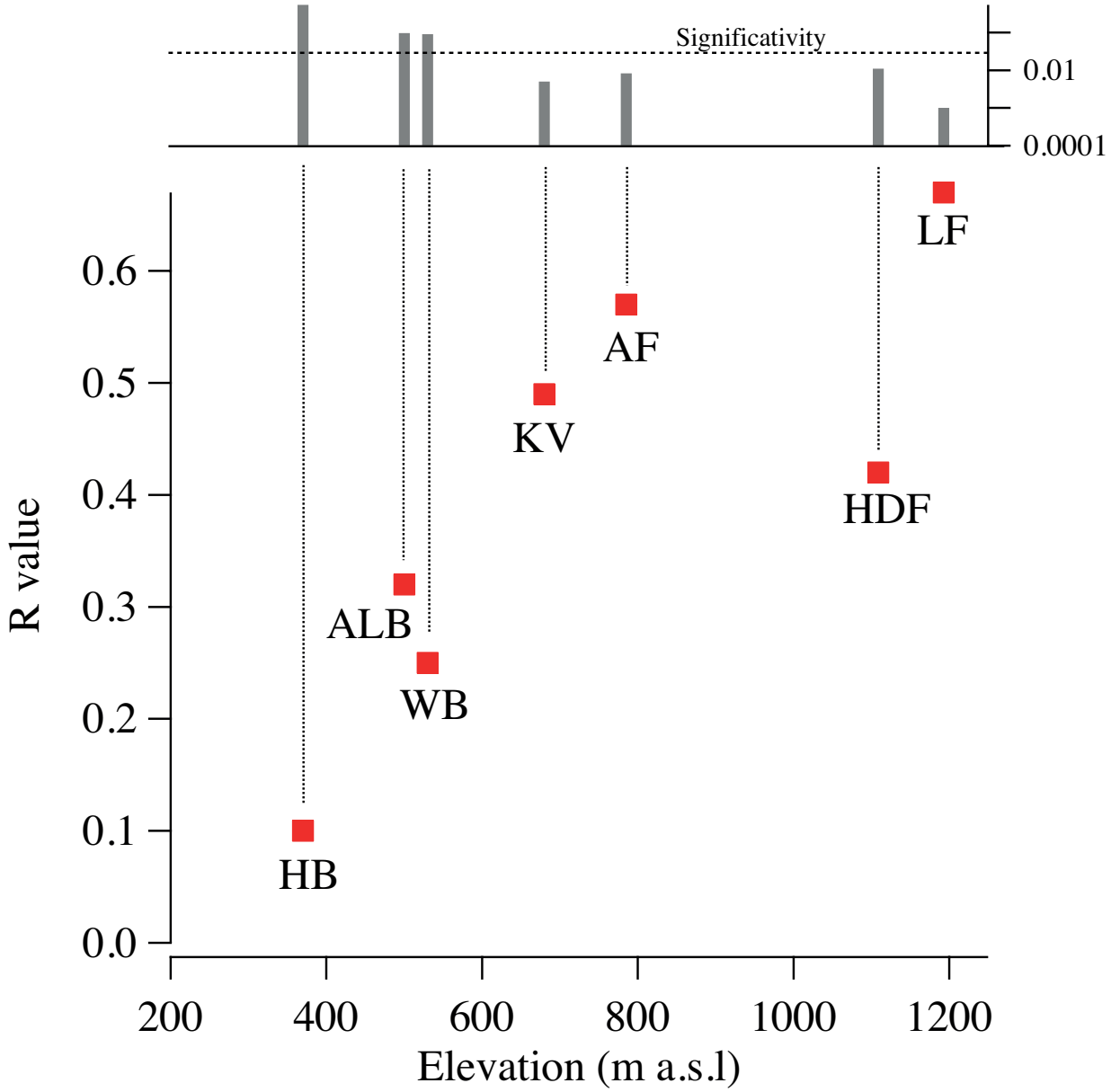

TABLES

Table 1. Table 1. Glaciers and sampling sites included in this study with their main characteristic. The air temperature was measured with a digital thermometer when the operators started to dig the snowpits. AWS: atmospheric weather station; UiO: University of Oslo; ThèMA: Thèoriser & Modèliser pour Amènager, University of Franche-Comté; NPI: Norwegian Polar Institute; IMAU: Institute for Marine and Atmospheric Research, Utrecht University; UoS: University of Silesia, IG PAS – Institute of Geophysics, Polish Academy of Sciences; CNR – Consiglio Nazionale delle Ricerche. Seven glaciers were considered at three different altitudes: 1) lower ablation zone; 2) ELA; 3) upper accumulation zone. Exceptionally, two snowpits (KVG 1 and KVG 1.5) were dug in the ablation zone of Kongsvegen glacier.

Table 2. Total load (mg m^{-2}) of major ions, calculated as the sum of loads in all layers of each snowpit. Sea salt sulphate (ss-SO_4^{2-}) and non-sea-salt sulphate (nss-SO_4^{2-}) are expressed as mg m^{-2}, while chloride depletion (Cl^-_{dep}) is given as a percentage and bromide enrichment (Br_{enr}) refers to an enrichment compared to seawater composition.

Table 3. Volume-weighted mean concentrations of major ions in each snowpit (calculated as the sum of loads in all layers divided by the total SWE of the snowpit): the nss (non-sea-salt) fractions have been calculated in each layer before the volume-weighting procedure. Average SWE-weighted stable water isotope ratios ($\delta^{18}O$ and δ^2H expressed as ‰) and average deuterium excess (*d*) are also reported.

Table 4. Loads (mg m^{-2}) of selected major ions from the 2016 sampling and from earlier studies at Lomonosovfonna summit (LF3), corresponding to the concentrations given in Fig. 4.

Table 5. Spearman rank order correlations of a) ionic loads (mg m^{-2}) and b) SWE-weighted mean concentrations of major ions across all 7 glaciers (n = 22 locations). ns = non-significant correlations (*p*-value > 0.05). Ionic loads were calculated from all snowpit layers, while SWE-weighted mean concentrations were calculated by dividing the total ionic loads in each snowpit by its total SWE. Non-sea-salt (nss) components were estimated based from seawater ratios to Na^+ (for Ca^{2+} and SO_4^{2-} in mg L^{-1}, it was 0.038 and 0.252, respectively; Millero et al., 2008).

Table 1. Glaciers and sampling sites included in this study with their main characteristics. The air temperature was measured with a digital thermometer when the operators started to dig the snow pits. AWS: automatic weather station; UiO: University of Oslo; ThèMA: Thèoriser & Modèliser pour Amènager, Université de Franche-Comté; NPI: Norwegian Polar Institute; IMAU: Institute for Marine and Atmospheric Research, Utrecht University; UoS: University of Silesia, IG PAS – Institute of Geophysics, Polish Academy of Sciences; CNR – Consiglio Nazionale delle Ricerche.

Glacier	**Site**	**Zone**	**AWS**	**Lat.** (°N)	**Lon.** (°E)	**Elev.** (m)	**Date** (dd.mm.yyyy)	**Air Temp.** (°C)	**Snow height** (cm)	**Snow Water Equivalent (SWE)** (mm)
Austfonna	AF1	ablation	UiO	79.734	22.414	336	21.04.2016	-13.5	106	330.50
	AF2	equilibrium line		79.767	22.825	507	23.04.2016	-7.1	135	439.59
	AF3	accumulation		79.832	24.004	785	24.04.2016	-14.7	181	803.93
Austre Lovénbreen	ALB1	ablation	ThéMA \CNR \NPI	78.883	12.136	195	25.04.2016	-3.7	81	296.66
	ALB2	equilibrium line		78.889	12.159	340	25.04.2016	-2.8	90	353.17
	ALB3	accumulation		78.861	12.187	513	20.04.2016	-11.3	161	499.67
Kongsvegen	KVG1	ablation	NPI\CNR	78.830	12.759	226	13.04.2016	-13.9	20	51.29
	KVG1.5	ablation		78.813	12.869	326	13.04.2016	-13.9	75	261.94
	KVG 2	equilibrium line		78.780	13.153	534	11.04.2016	-17.5	162	575.78
	KVG3	accumulation		78.756	13.336	672	12.04.2013	-15.5	234	880.13
Holtedahlfonna	HDF1	ablation	NPI\CNR	78.931	13.303	570	17.04.2016	-14.5	108	372.98
	HDF2	equilibrium line		79.029	13.531	718	17.04.2016	-14.2	175	625.00
	HDF3	accumulation		79.140	13.394	1119	15.04.2016	-18.1	201	732.08
Lomonosovfonna	LF1	ablation	IMAU	78.633	17.077	223	10.04.2016	-10.9	27	99.4
	LF2	equilibrium line		78.691	17.150	523	9.04.2016	-5.8	94	277.28
	LF3	accumulation		78.824	17.435	1193	11.04.2016	-24	146	487.01
Hansbreen	HB1	ablation	UoS/IG PAS	77.049	15.639	102	25.04.2016	-7.3	102	396.10
	HB2	equilibrium line		77.083	15.639	275	25.04.2016	-6.9	169	640.28
	HB3	accumulation		77.120	15.487	396	29.04.2016	0.7	288	1305.09
Werenskiöldbreen	WB1	ablation	UoS	77.075	15.313	166	16.04.2016	-9.2	81	328.34
	WB2	equilibrium line		77.072	15.441	413	16.04.2016	-11.2	110	454.75
	WB3	accumulation		77.092	15.489	528	18.04.2016	-11.1	330	1396.60

Table 2. Total load (mg m^{-2}) of major ions, calculated as the sum of loads in all layers of each snow pit. Sea-salt sulphate (ss-SO_4^{2-}) and non-sea-salt sulphate (nss-SO_4^{2-}) are expressed as mg m^{-2}, while chloride depletion (Cl^-_{dep}) is given as a percentage and bromide enrichment (Br_{enr}) refers to an enrichment compared to seawater.

Site	Cl^-	Br^-	SO_4^{2-}	NO_3^-	Na^+	NH_4^+	K^+	Mg^{2+}	Ca^{2+}	ss-SO_4^{2-}	nss-SO_4^{2-}	Cl^-_{dep} %	Br_{enr}
KVG1	190	0.4	96	6	421	0.3	7	37	20	106	nd	75	0.2
KVG1.5	281	1.9	157	45	327	0.9	6	36	33	82	75	52	1.0
KVG2	652	1.2	342	118	605	1.9	9	51	63	152	190	40	0.3
KVG3	1039	1.2	509	148	967	2.9	12	86	94	244	266	40	0.2
HDF1	373	1.3	144	74	267	2.6	4	23	33	68	79	21	0.9
HDF2	423	2.5	192	148	240	4.5	6	18	67	61	131	2	1.7
HDF3	227	0.8	65	51	170	4.5	9	12	45	43	22	25	0.8
ALB1	446	1.9	226	115	343	1.5	10	31	90	86	139	27	0.9
ALB2	294	1.4	158	87	221	1.6	4	17	38	56	107	25	1.2
ALB3	729	1.8	342	64	648	4.2	8	56	81	158	165	36	0.4
LF1	75	1.1	59	1	95	0.4	3	12	6	31	48	51	2.1
LF2	174	2.8	127	18	141	2.6	5	12	7	53	127	38	3.2
LF3	216	3.5	144	10	225	2.9	7	22	9	56	93	45	2.7
AF1	498	5.7	348	38	578	2.2	27	48	95	127	173	53	1.6
AF2	438	6.3	263	15	509	3.4	19	62	26	147	153	51	2.0
AF3	928	6.5	439	88	933	8.1	35	89	81	185	206	54	1.5
WB1	2041	4.7	332	34	1278	6.7	53	131	91	340	15	10	0.6
WB2	1584	2.7	304	38	1051	9.9	44	110	68	220	24	16	0.4
WB3	3922	7.2	713	118	2649	26.1	137	277	313	671	37	17	0.5
HB1	2680	6.2	482	46	1722	10.5	74	201	110	475	47	13	0.6
HB2	2499	2.8	490	185	1667	32.5	105	159	150	350	73	19	0.3
HB3	3964	6.5	719	118	2557	28.2	125	281	223	751	107	13	0.4

Table 3. Volume-weighted mean concentrations of major ions in each snow pit (calculated as the sum of concentrations in all layers divided by the total SWE of the snow pit): the nss (non-sea-salt) fractions were calculated in each layer before the volume-weighting procedure. Average SWE-weighted stable water isotope ratios ($\delta^{18}O$ and δ2H expressed as ‰) and average deuterium excess (*d*) are also reported.

Site	Cl^-	Br^-	SO_4^{2-}	NO_3^-	Na^+	NH_4^+	K^+	Mg^{2+}	Ca^{2+}	nss-SO_4^{2-}	nss- K^+	nss- Mg^{2+}	nss-Ca^{2+}	$\delta^{18}O$	δ2H	d
KVG1	3.71	0.008	1.88	0.12	8.21	0.005	0.15	0.716	0.384	(-0.19)	(-0.16)	(-0.26)	0.07	-9.69	-66.17	11.37
KVG1.5	1.07	0.007	0.60	0.17	1.25	0.004	0.01	0.139	0.126	0.29	(-0.02)	(-0.01)	0.08	-11.32	-78.25	12.34
KVG2	1.13	0.002	0.60	0.21	1.05	0.003	0.02	0.088	0.109	0.33	(-0.02)	(-0.04)	0.07	-12.51	-88.62	11.48
KVG3	1.18	0.001	0.58	0.17	1.10	0.003	0.01	0.098	0.107	0.30	(-0.03)	(-0.03)	0.07	-12.72	-89.50	12.25
HDF1	1.03	0.004	0.39	0.21	0.72	0.007	0.01	0.062	0.098	0.21	(-0.02)	(-0.02)	0.07	-13.51	-94.37	13.75
HDF2	0.68	0.004	0.31	0.24	0.39	0.007	0.01	0.029	0.108	0.21	(-0.01)	(-0.02)	0.09	-13.91	-99.15	12.10
HDF3	0.31	0.001	0.09	0.07	0.23	0.006	0.01	0.016	0.062	0.03	0.00	(-0.01)	0.05	-15.18	-104.51	16.97
ALB1	1.50	0.007	0.76	0.39	1.16	0.005	0.04	0.106	0.304	0.47	(-0.01)	(-0.03)	0.25	-11.22	-75.17	14.59
ALB2	0.84	0.005	0.46	0.27	0.63	0.005	0.01	0.049	0.116	0.30	(-0.01)	(-0.03)	0.09	-12.19	-83.11	14.40
ALB3	1.43	0.003	0.65	0.12	1.25	0.006	0.01	0.107	0.161	0.33	(-0.03)	(-0.04)	0.11	-12.40	-85.40	13.79
LF1	1.09	0.016	0.80	0.06	1.250	0.012	0.040	0.143	0.076	0.48	(-0.006)	(-0.006)	0.028	-11.61	-82.79	10.10
LF2	0.84	0.015	0.65	0.07	0.753	0.013	0.027	0.065	0.044	0.46	(-0.001)	(-0.024)	0.015	-14.54	-105.44	10.90
LF3	0.45	0.007	0.31	0.02	0.456	0.006	0.014	0.043	0.015	0.19	(-0.003)	(-0.012)	-0.003	-15.14	-110.42	10.69
AF1	1.28	0.014	0.91	0.10	1.524	0.005	0.070	0.110	0.278	0.52	0.013	(-0.072)	0.220	-14.34	-100.76	13.94
AF2	1.16	0.016	0.68	0.03	1.331	0.008	0.052	0.170	0.069	0.35	0.003	0.012	0.018	-16.00	-111.15	16.84
AF3	0.76	0.008	0.49	0.11	0.914	0.011	0.034	0.081	0.090	0.26	0.000	(-0.028)	0.055	-13.89	-96.89	14.24
WB1	6.596	0.014	1.079	0.105	4.12	0.02	0.18	0.43	0.27	0.05	0.02	(-0.05)	0.11	-10.17	-70.62	10.75
WB2	2.886	0.005	0.536	0.066	1.92	0.01	0.07	0.19	0.14	0.05	0.00	(-0.04)	0.07	-10.25	-70.14	11.90
WB3	2.824	0.005	0.506	0.086	1.91	0.02	0.10	0.20	0.17	0.03	0.03	(-0.03)	0.10	-9.54	-63.64	12.66
HB1	7.378	0.016	1.316	0.127	4.76	0.03	0.20	0.57	0.49	0.12	0.02	0.01	0.31	-11.14	-75.93	13.19
HB2	3.155	0.004	0.661	0.283	2.17	0.04	0.12	0.19	0.21	0.11	0.04	(-0.07)	0.13	-10.69	-73.34	12.17
HB3	3.573	0.005	0.658	0.098	2.28	0.03	0.12	0.26	0.19	0.08	0.04	(-0.02)	0.10	-11.25	-77.62	12.35

Table 4. Loads (mg m^{-2}) of selected major ions from the 2016 sampling and from earlier studies at Lomonosovfonna summit (LF3), corresponding to the concentrations given in Fig. 4.

Year	Na^+	Ca^{2+}	NO_3^-	nss-SO_4^{2+}	Study
2002	126.7	7.1	27.3	37.1	(Virkkunen et al., 2007)
2009	n.a.	n.a.	33.5	n.a.	*Vega C. (unpublished data)*
2010	80.1	24.3	52.3	48.1	*Vega C. (unpublished data)*
2011	262.9	46.2	27.2	34.1	(Vega et al., 2015)*, Vega C.(unpublished data)*
2016	222.2	7.2	11.4	93.0	*This study*

Table 5. Spearman rank order correlations of a) ionic loads (mg m^{-2}) and b) SWE-weighted mean concentrations of major ions across all 7 glaciers (n=22 locations). ns = non-significant correlations (*p*-value > 0.05). Ionic loads were calculated from all snow pit layers, while SWE-weighted mean concentrations were calculated by dividing the ionic loads in each snow pit by its total SWE. Non-sea-salt (nss) components were estimated based from seawater ratios to Na^+ (0.038 and 0.252, respectively, for Ca^{2+} and SO_4^{2-} in mg L^{-1} ; Millero et al., 2008).

a)

	Cl^-	Br^-	SO_4^{2-}	NO_3^-	Na^+	NH_4^+	K^+	Mg^{2+}	Ca^{2+}	nss-SO_4^{2-}
Br^-	0.53									
SO_4^{2-}	0.93	0.60								
NO_3^-	0.55	ns	0.55							
Na^+	0.94	0.48	0.92	0.44						
NH_4^+	0.73	0.62	0.68	ns	0.64					
K^+	0.82	0.61	0.81	ns	0.85	0.75				
Mg^{2+}	0.90	0.51	0.88	ns	0.98	0.62	0.82			
Ca^{2+}	0.86	ns	0.83	0.69	0.82	0.61	0.76	0.71		
nss-SO_4^{2-}	ns	ns	ns	ns	ns	ns	ns	ns	ns	ns
nss-Ca^{2+}	0.76	ns	0.75	0.77	0.68	0.56	0.66	0.56	0.96	ns

b)

	Cl^-	Br^-	SO_4^{2-}	NO_3^-	Na^+	NH_4^+	K^+	Mg^{2+}	Ca^{2+}	nss-SO_4^{2-}
Br^-	ns									
SO_4^{2-}	0.75	0.58								
NO_3^-	ns	-0.48	ns							
Na^+	0.95	ns	0.80	ns						
NH_4^+	ns	ns	ns	ns	0.47					
K^+	0.83	0.46	0.73	ns	0.88	0.62				
Mg^{2+}	0.92	ns	0.78	ns	0.98	0.47	0.86			
Ca^{2+}	0.85	ns	0.64	0.44	0.76	ns	0.62	0.70		
nss- SO_4^{2-}	ns	ns	ns	ns	ns	ns	ns	ns	ns	ns
nss-Ca^{2+}	0.67	ns	0.45	0.56	0.54	ns	ns	0.47	0.91	ns